Cell



# PABP/purine-rich motif as an initiation module for cap-independent translation in pattern-triggered immunity

## Graphical abstract

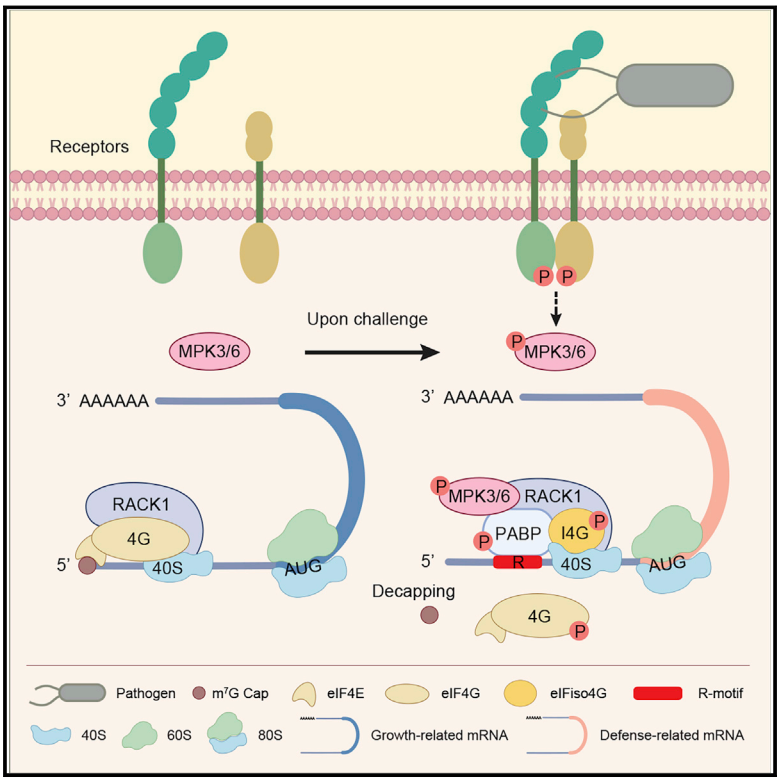


## Highlights

- PTI induces mRNA decapping and defense mRNA translation using R-motif as an IRES
- PABPs activate R-motif-mediated translation by association with eIFiso4G over eIF4G
- MPK3/6 phosphorylate eIF4G, PABP, and eIFiso4G using RACK1 as a scaffold during PTI
- Phosphorylation inhibits eIF4G while activating PABP/eIFiso4G-mediated translation

## Authors

Jinlong Wang, Xing Zhang, George H. Greene, Guoyong Xu, Xinnian Dong

## Correspondence

xdong@duke.edu

## In brief

Study of the pattern-triggered immunity (PTI) signaling pathway unveils a cap-independent translation mechanism for facilitating stress-induced translatome reprogramming.

Wang et al., 2022, Cell *185*, 3186–3200
August 18, 2022 
https://doi.org/10.1016/j.cell.2022.06.037

CellPress

CellPress
OPEN ACCESS

Cell

Article

# PABP/purine-rich motif as an initiation module for cap-independent translation in pattern-triggered immunity

Jinlong Wang,[1,2] Xing Zhang,[1,2] George H. Greene,[1,2,3] Guoyong Xu,[1,2,4] and Xinnian Dong[1,2,5,*]
[1]Howard Hughes Medical Institute, Duke University, Durham, NC 27708, USA
[2]Department of Biology, Duke University, Durham, NC 27708, USA
[3]Present address: Upstream Biotechnology Inc., Durham, NC 27701, USA
[4]Present address: State Key Laboratory of Hybrid Rice, Institute for Advanced Studies (IAS), Wuhan University, Wuhan, Hubei 430072, China
[5]Lead contact
*Correspondence: xdong@duke.edu
https://doi.org/10.1016/j.cell.2022.06.037

## SUMMARY

Upon stress, eukaryotes typically reprogram their translatome through GCN2-mediated phosphorylation of the eukaryotic translation initiation factor, eIF2α, to inhibit general translation initiation while selectively translating essential stress regulators. Unexpectedly, in plants, pattern-triggered immunity (PTI) and response to other environmental stresses occur independently of the GCN2/eIF2α pathway. Here, we show that while PTI induces mRNA decapping to inhibit general translation, defense mRNAs with a purine-rich element (“R-motif”) are selectively translated using R-motif as an internal ribosome entry site (IRES). R-motif-dependent translation is executed by poly(A)-binding proteins (PABPs) through preferential association with the PTI-activating eIFiso4G over the repressive eIF4G. Phosphorylation by PTI regulators mitogen-activated protein kinase 3 and 6 (MPK3/6) inhibits eIF4G’s activity while enhancing PABP binding to the R-motif and promoting eIFiso4G-mediated defense mRNA translation, establishing a link between PTI signaling and protein synthesis. Given its prevalence in both plants and animals, the PABP/R-motif translation initiation module may have a broader role in reprogramming the stress translatome.

## INTRODUCTION

Most eukaryotic mRNAs are translated in the canonical cap-dependent manner (Hinnebusch et al., 2016; Jackson et al., 2010). To initiate translation, the ternary complex (eIF2-GTP-Met-tRNAi) is loaded onto the 40S ribosomal subunit to form the 43S preinitiation complex (PIC), which is then recruited to the $m^7$G-capped 5′ end of an mRNA through the eIF4F complex, composed of the cap-binding protein eIF4E, the scaffold protein eIF4G, and the RNA helicase eIF4A. The recruitment of 43S PIC to the 5′ cap is facilitated by the poly(A)-binding protein (PABP), which loops back from the 3′ poly(A) tail of the mRNA by interacting with eIF4G in the eIF4F complex (Kahvejian et al., 2001; Wells et al., 1998). In response to stress, general translation initiation is often inhibited through stress-induced phosphorylation of eIF2α, which reduces the availability of the active ternary complex. Certain stress-responsive mRNAs, such as general control nondepressible 4 (*GCN4*) in yeast and activating transcription factor 4 (*ATF4*) in mammals, whose translation is normally inhibited by the upstream open reading frames (uORFs) in their mRNAs, are preferentially translated at the reduced level of the ternary complex (Echevarría-Zomeño et al., 2013). However, in plants, although eIF2α phosphorylation is noted during many stress responses including pattern-triggered immunity (PTI) (Izquierdo et al., 2018; Lokdarshi et al., 2020; Pajerowska-Mukhtar et al., 2012; Xu et al., 2017), blocking this process in the *GCN2* mutant has no effect on the responses to biotic and abiotic stresses (Izquierdo et al., 2018; Lokdarshi et al., 2020; Xu et al., 2017) with one observed exception (Liu et al., 2019). This begs the question: how do plants repress the translation of growth-related proteins while selectively translating defense proteins in response to biotic and abiotic stresses?

In our previous study of the PTI translatome, a purine-rich element, “R-motif,” was found to be highly enriched in the 5′ leader sequences of mRNAs with enhanced translational efficiency and to play an essential role in regulating defense protein translation through interaction with PABPs (Xu et al., 2017). However, the signaling pathway from the perception of microbe-associated molecular patterns (MAMPs) by the pattern-recognition receptors (PRRs) to the PABP/R-motif module and the molecular mechanism by which the translatome is reprogrammed for defense remain unknown.

In this study, we report that upon perception of the MAMP, elf18 (N-terminal epitope of the bacterial elongation factor Tu),

 

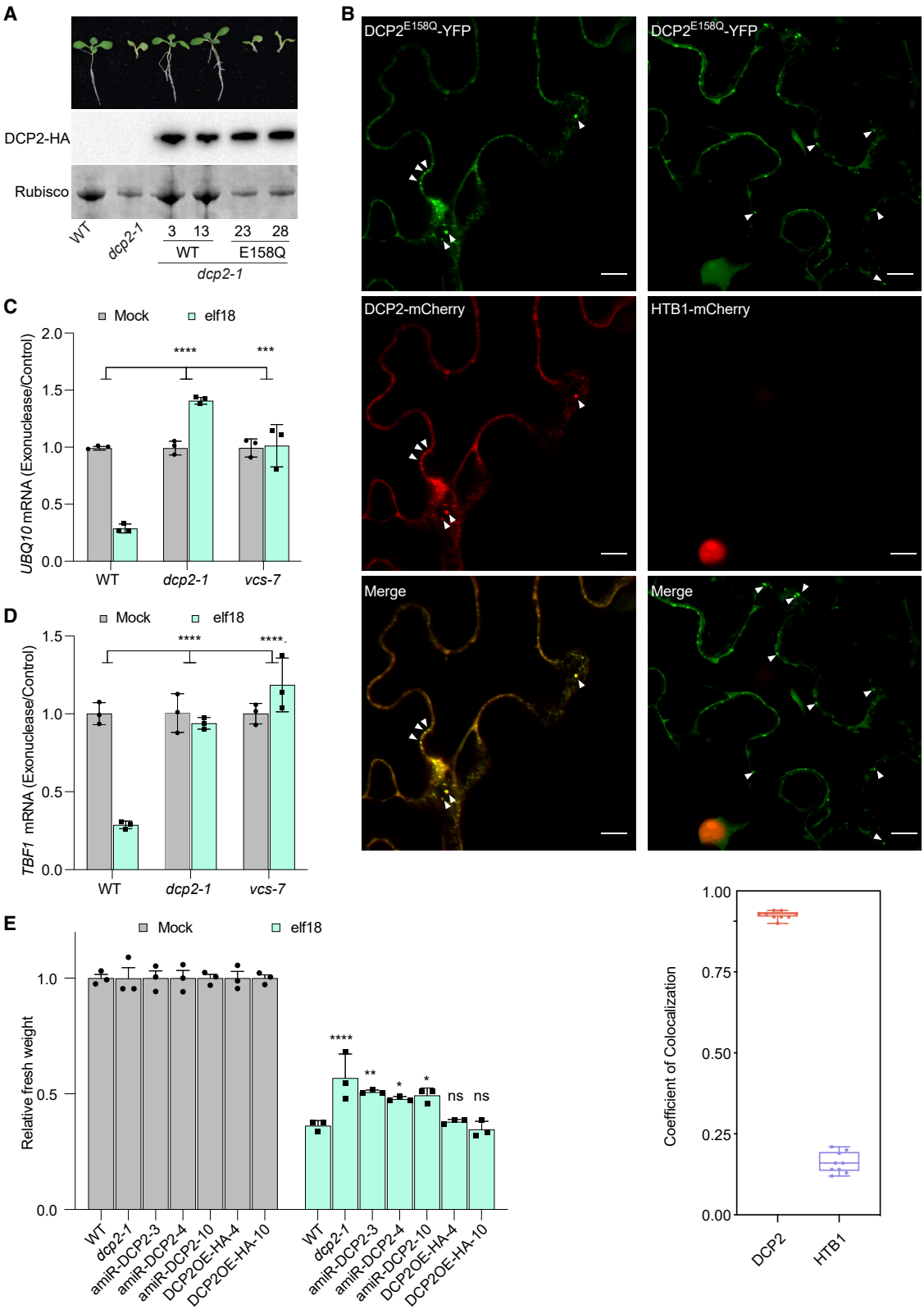


(legend on next page)

there is an increase in decapping activity by the decapping protein (DCP) to inhibit the canonical cap-dependent translation. mRNAs with the R-motif use this sequence as a cap surrogate for internal ribosome entry to promote defense protein translation by recruiting PABPs and their differential associations with eIF4G and eIFiso4G. Although PABP-associated eIF4G represses basal resistance, its isomer eIFiso4G facilitates elf18-triggered immunity. Moreover, we demonstrate that the switch from canonical cap-dependent translation to R-motif-mediated translation is triggered by the key PTI regulators MPK3/6 through phosphorylation of PABP, eIF4G, and eIFiso4G with receptor for activated C kinase 1 (RACK1) as a scaffold.

## RESULTS

### Elf18-induced mRNA decapping by the DCP complex positively affects PTI

To determine how elf18 induces translational reprogramming, we first tested the decapping process, catalyzed by the enzyme decapping 2 (DCP2) along with its co-activator DCP1 and the scaffold protein varicose (VCS) (Figure S1A), which is known to control mRNA turnover (Yu et al., 2019). We generated transgenic lines overexpressing either the wild-type (WT) DCP2 or the decapping-deficient variant, DCP2$^{E158Q}$ (Xu et al., 2006), in the *dcp2-1* mutant. We found that the WT DCP2 rescued the growth defect of the mutant, whereas DCP2$^{E158Q}$ failed to do so (Figure 1A). Since DCPs also serve as core components of processing bodies (P-bodies) (Xu et al., 2006), we imaged YFP-tagged DCP2$^{E158Q}$ to determine its effect on P-body formation. We found that the E158Q mutant protein colocalized with the WT DCP2 (Figure 1B), indicating that the phenotype of the *dcp2-1* allele is less likely caused by a deficiency in P-body formation than the deficiency in mRNA decapping known for the DCP2$^{E158Q}$ mutant.

We then used the *dcp2-1* mutant to determine whether decapping occurs upon PTI induction and whether it is a selective process to target non-defense mRNAs. We performed the exonuclease sensitivity assay on mRNAs extracted from mock- and elf18- treated WT, *dcp2-1* and *vcs-7* mutant plants to measure the decapping activity. We found that the housekeeping gene *ubiquitin 10* (*UBQ10*) indeed became sensitive to the exonuclease digestion upon elf18 induction in WT plants but not in the decapping mutants (Figure 1C). Surprisingly, mRNAs of *TL1-binding transcription factor 1* (*TBF1*), encoding a key positive immune regulator (Pajerowska-Mukhtar et al., 2012), and eight other R-motif-containing defense genes (Table S1), all became more sensitive to exonuclease digestion in a DCP-dependent manner (Figures 1D and S1B–S1I). This conclusion was further confirmed by quantifying mRNAs immunoprecipitated by an antibody against the cap structure before and after elf18 treatment (Figures S1J and S1K).

We next tested whether this elf18-triggered mRNA decapping plays a role in PTI by generating transgenic lines with an inducible artificial microRNA (amiRNA) to transiently knockdown *DCP2* (Schwab et al., 2006) without the growth defect observed in the *dcp2-1* mutant (Figure 1A). Quantitative PTI-induced seedling growth inhibition was used as a readout because it likely results from translatome reprogramming. We found all the amiRNA lines partially compromised in elf18-induced plant growth inhibition similarly to the *dcp2-1* mutant, whereas the DCP2-HA overexpressing lines (DCP2OE-HA) had no detectible effect (Figure 1E), consistent with a previous report (Yu et al., 2019). Together, these findings demonstrate that elf18-triggered decapping of mRNAs by the DCP complex contributes positively to PTI, possibly by diminishing canonical translational activity required for plant growth.

### R-motif recruits PABP to regulate cap-independent protein translation

Since PTI-induced decapping is not specific to growth-related mRNAs, we asked how defense proteins are selectively translated during PTI independently of the cap structure. Our previous study identified a highly enriched purine-rich mRNA consensus sequence, R-motif, in the 5′ leader sequences of mRNAs with increased translational efficiency upon PTI induction (Xu et al., 2017). We hypothesized that the R-motif might function as an internal ribosome entry site (IRES) to mediate cap-independent translation of key defense proteins. To test this hypothesis, we used a translational firefly luciferase (FLUC) reporter driven by the *TBF1* 5′ leader sequence. Our previous studies showed that immune-induced translation of *TBF1* is regulated by its 5′ leader sequence containing one R-motif and two uORFs (Pajerowska-Mukhtar et al., 2012; Xu et al., 2017). Re-analysis of the sequence led to the discovery of two additional R-motifs, R2 and R3, located between and downstream of uORF1 and uORF2, respectively (Figure S2A). To determine whether mutating these R-motifs affects *TBF1* translation, we made the ''dual luciferase'' reporters with the constitutively expressed renilla luciferase, *35S:RLUC*, as an internal control for the reporter containing either WT *35S:uORF/R$_{TBF1}$-FLUC* or the R-motif mutants (*mRs*) *35S:uORFs/mRs$_{TBF1}$-FLUC* (Table S2). The reporters were either stably

**Figure 1. Elf18-induced mRNA decapping by the DCP complex positively affects PTI**

(A) Independent transgenic plants expressing *35S:DCP2-HA* (WT)(3, 13) and *35S:DCP2$^{E158Q}$-HA* (E158Q)(23, 28) in *dcp2-1* (top panel) with similar expression levels (middle panel) and Rubisco as a loading control (bottom panel). Representative seedlings were photographed after 10 days on ½ MS.

(B) Confocal images of P-body colocalization of DCP2-mCherry and DCP2$^{E158Q}$-YFP transiently expressed in *Nb* plants. Histone H2B (HTB)-mCherry, negative control. Colocalization coefficient was based on 9 images (bottom graph). Data are presented as box-and-whisker plot. Scale bars, 10 μm.

(C and D) Elf18-induced decapping of *UBQ10* (C) and *TBF1* (D) mRNAs was measured using 8-day-old seedlings after mock or 10 μM elf18 for 1 h and exposed to exonuclease before qPCR. Values are means ± SDs after normalizing to the unexposed control.

(E) Elf18-induced growth inhibition. 5-day-old seedlings were treated with or without 50 μM estradiol overnight, followed by mock or 100 nM elf18 for 3–4 days before fresh weight was measured. amiR-DCP2-3, -4, and -10 and DCP2OE-4, and -10, independent transgenic lines expressing estradiol-inducible artificial microRNA against *DCP2* and overexpressing *DCP2*, respectively. Values are means ± SDs.

Each dot represents a biological replicate. Data were analyzed via two-way ANOVA (C and D) and two-way ANOVA with Dunnett multiple comparisons (E), *p < 0.05, **p < 0.01, ***p < 0.001, ****p < 0.0001. ns, not significant. See also Figure S1.

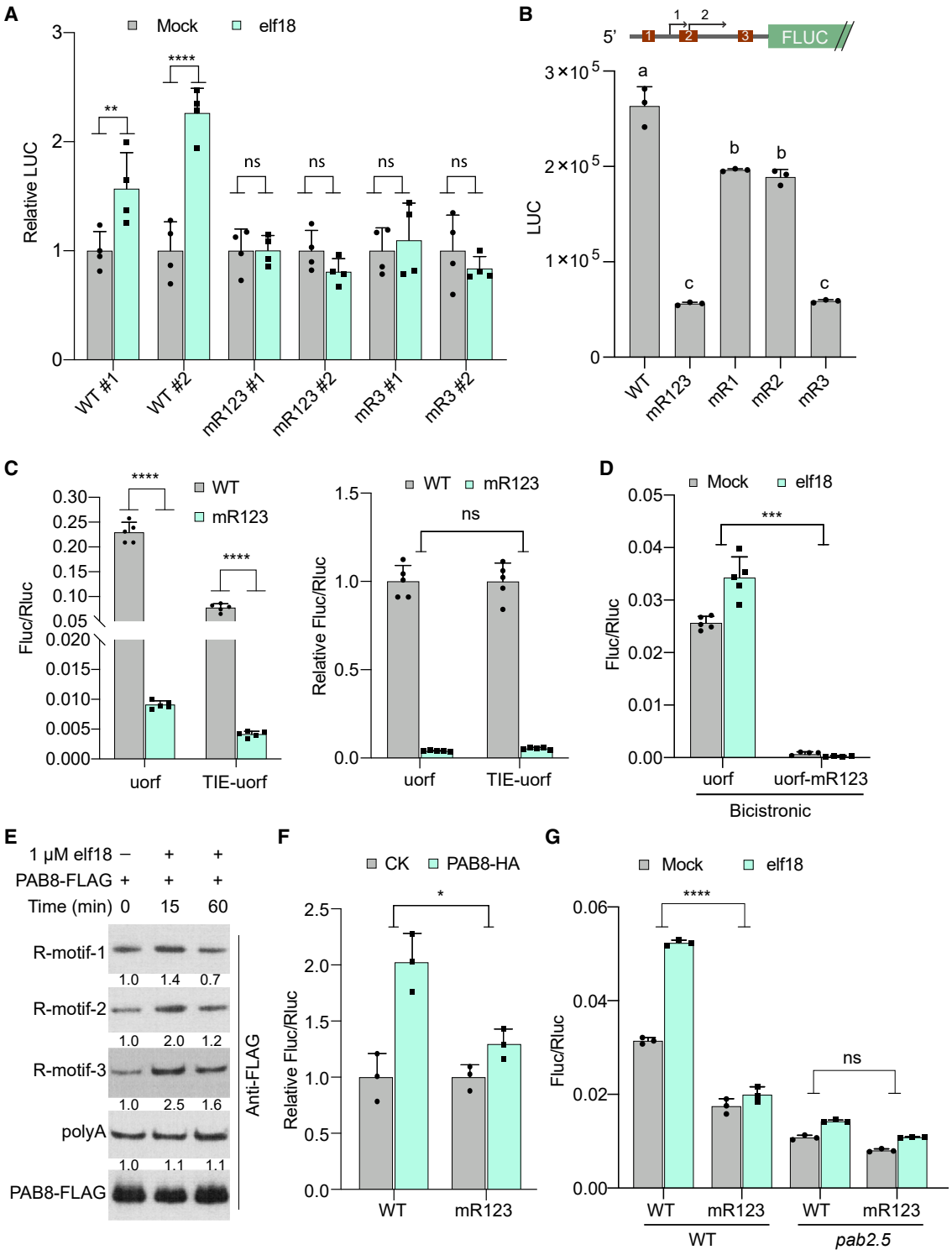


**Figure 2. PABPs are required for R-motif-mediated cap-independent protein translation**

(A) *In planta* elf18-induced translation of *TBF1* dual luciferase reporters with WT or mutated R-motifs (*mRs*). 3- to 4-week-old independent *Arabidopsis* transgenic lines carrying the reporters were sprayed with 2 mM luciferin overnight before infiltrating with mock (water) or 10 μM elf18 for 1 h. Luciferase activity was measured using a CCD camera with 20-min exposure time. Values are means ± SDs.

*(legend continued on next page)*

transformed into *Arabidopsis* plants or transiently expressed in *Nicotiana benthamiana* (*Nb*). We found that mutating the R-motifs, especially R2 and R3, greatly diminished the elf18-induced reporter translation (Figures 2A and S2B) but not the reporter mRNA abundance (Figure S2C), suggesting that R-motifs positively regulate defense-related mRNA translation during PTI. We then performed *in vitro* translation assays using the *TBF1* reporter mRNAs without the 5′ cap and found that mutating any of the three R-motifs decreased the level of translation compared with WT (Figure 2B), indicating that R-motifs in the *TBF1* 5′ leader sequence could facilitate translation independently of the cap, perhaps as a cap surrogate in recruiting ribosome. To test whether addition of the cap structure to the *TBF1* reporter would affect R-motifs' activity, we used the uORF1 and uORF2 mutant, *uorf*, to remove the effect of cap-dependent regulation of uORFs on the reporter. We found that although addition of the cap enhanced translation in the *in vitro* system, the fold increases in the translational activities caused by capping the *uorf* and *uorf/mR123* reporter mRNAs were similar, indicating that the R-motif contributes positively to translation, regardless of the presence of the cap (Figure S2D), supporting our hypothesis that R-motif-mediated translation is cap-independent.

To confirm that R-motif functions as an IRES *in planta*, we took two different approaches. First, we used a translation inhibitory element (TIE) found in a mammalian gene to block cap-dependent translation (Xue et al., 2015) by adding it to the 5′ end of the *TBF1* leader sequence (*uorf*) in the luciferase reporters and transiently expressed them in *Nb* plants. We found that compared with the drastic reduction in the reporter activity by mutating R-motifs, the addition of *TIE* to *uorf* and *uorf/mR123* caused similar fold reductions in reporter activities (Figure 2C), indicating that R-motif-mediated translation is cap-independent. Second, we constructed bicistronic reporters in which the *uorf* or *uorf/mR123* leader sequence of *TBF1* was inserted between the first cistron *RLUC* and the second cistron *FLUC*. From the same mRNA, the 5′ *RLUC* is translated through cap-dependent initiation and serves as an internal control, although the 3′ *FLUC* is expected to be translated only if the *TBF1* 5′ leader sequence contains an IRES. We found that when transiently expressed in *Nb* plants, translational activities observed in the *uorf* reporter were diminished in the *uorf/mR123* reporter (Figure 2D), supporting our hypothesis that R-motif is a cellular IRES.

We next sought to explore the underlying mechanisms of R-motif-mediated protein translation during PTI. Our previous study showed that PABPs (PAB2, PAB4, and PAB8) can bind to synthetic GA-rich RNA probes (GA × 60, G[A]3 × 30, and G[A]6 × 20) *in vitro* (Xu et al., 2017), making them promising candidates in mediating R-motif-dependent translation. To test this hypothesis, we used biotin-conjugated RNA probes containing *TBF1* R-motifs and incubated them with PAB8-FLAG purified from protoplasts with or without elf18 treatment. Immunoblot analysis showed that all three probes interacted with the PAB8-FLAG protein, and the interactions were transiently increased following elf18 treatment compared with the poly(A) control whose interaction with PAB8-FLAG remained unchanged (Figure 2E), indicating that PABP binding to R-motifs is dynamically regulated during PTI. Next, we coexpressed PAB8-HA with either the WT or the R-motif mutant (*mR123*) dual luciferase reporters in *Nb* plants to test the effects of PABPs on the reporter translation. The results showed that at comparable reporter mRNA and PAB8-HA protein levels (Figures S2E and S2F), PAB8-HA significantly promoted the WT, but not the *mR123*, reporter translation (Figure 2F), consistent with our hypothesis that PABPs can regulate protein translation through binding to the R-motif. Tethering experiment (Bertrand et al., 1998) demonstrates that recruitment of PABPs to the 5′ leader sequence is sufficient to initiate translation in the absence of R-motif (Figure S2G). To further confirm the role of PABPs in R-motif-mediated translation genetically, we transiently expressed the WT reporter into protoplasts made from WT or the *pab2.5* (*pab2 pab8 pab4*$^{+/-}$) mutant and found that the elf18-induced translation was similarly compromised in *pab2.5* as the *mR123* reporter (Figure 2G), supporting the role of PABPs in regulating protein translation through dynamic association with R-motif.

## PABPs reprogram defense protein translation through differential associations with eIF4G and eIFiso4G

Previous work in yeast showed that PABPs have a redundant function with the eIF4E in mediating protein translation (Tarun and Sachs, 1995; Tarun et al., 1997), suggesting that PABPs

(B) *In vitro* translation of uncapped *TBF1* reporter mRNAs with WT or mutated R-motifs. Top, a schematic of mRNA carrying the *TBF1* 5′ leader sequence (3 R-motifs and 2 uORFs [arrows]) and the N-terminal 12 amino acid coding sequence of *TBF1* fused with the firefly luciferase gene (*FLUC*). Bottom, translation activities (FLUC) of the mRNAs measured using the wheat-germ translation system. Values are means ± SDs.

(C) *In planta* translation of *TBF1* dual luciferase reporters with mutated uORFs (*uorf*) and with or without a 5′ translation inhibitory element (*TIE*). The reporters were transiently expressed in *Nb* plants for 20 h before the luciferase activities were measured. Values are means ± SDs.

(D) *In planta* translation of *TBF1* bicistronic reporters. The *35S:RLUC-uorf/R*$_{TBF1}$*-FLUC* (Bicistronic-*uorf*) or the *35S:RLUC-uorf/mR123*$_{TBF1}$*-FLUC* mutant (Bicistronic-*uorf/mR123*) reporter was transiently coexpressed with the elf18 receptor EFR-GFP in *Nb* plants for 20 h and infiltrated with 10 μM elf18 or water for 2 h before the luciferase activities were measured. Values are means ± SDs.

(E) Pulldown of PABPs by biotinylated *TBF1* R-motifs or polyA sequence. PAB8-FLAG protein was purified from protoplasts treated with 1 μM elf18 for the indicated time, and the protein was quantified by immunoblotting using an anti-FLAG antibody. Numbers under each blot are the ratios to time 0 after normalized to the input (bottom blot).

(F) The effect of PAB8-HA on the translational activities of *TBF1* dual luciferase reporters. Reporter activities were determined 2 days after transient coexpression in *Nb* plants. Values are means ± SDs.

(G) The effect of PABP mutation on the *TBF1* dual luciferase reporter translation. The reporters were expressed overnight in protoplasts made from WT and the *pab2 pab8 pab4*$^{+/-}$ mutant (*pab2.5*) and treated with 1 μM elf18 for 45 min before luciferase activities were recorded. Values are means ± SDs.

Each dot represents a biological replicate. Data were analyzed via two-way ANOVA with Dunnett multiple comparisons (A), one-way ANOVA (Tukey) (B), t test (left C), and two-way ANOVA (right C, D, F, and G), *$p < 0.05$, **$p < 0.01$, ***$p < 0.001$, ****$p < 0.0001$. Different letters indicate statistical significance, $p < 0.05$. ns, not significant. See also Figure S2.

may serve as eIF4E alternates in recruiting other eIFs to the R-motif. To test this hypothesis, we performed liquid chromatography-tandem mass spectrometry (LC-MS/MS) analysis to identify PABP-interacting proteins and detected 10 eIFs and 13 other candidates that may function in the translation initiation process (Table S3). STRING (Search Tool for the Retrieval of Interacting Genes/Proteins) analysis showed that eIF4G and RACK1A are possible ''hub proteins'' mediating the interaction of PABPs with the translation initiation complex (Figure 3A). We first confirmed the PABP-eIF4G interaction using both the split-luciferase complementation assays in *Nb* plants (Figures S3A–S3C) as well as co-immunoprecipitation (coIP) in *Arabidopsis* protoplasts (Figures S3D and S3E). The plant-specific isomer of the canonical eIF4G, eIFiso4G1, also interacted with PABPs (Figures S3A–S3E). We then performed a time course experiment to trace the interaction dynamics of PABPs with eIF4G and eIFiso4G1 after treating *Nb* plants with elf18. Surprisingly, we found that following the elf18 treatment, PABPs' interactions with these proteins were initially reduced before recovering, with the PABPs/eIF4G pair showing a faster and more dramatic reduction and recovery than the PABPs/eIFiso4G1 pair (Figures 3B, S3F, and S3G), indicating that upon PTI induction, PABP may switch from canonical cap-dependent translation to R-motif-mediated cap-independent defense protein translation by transiently switching association from eIF4G to eIFiso4G.

To test this hypothesis, we examined the double-mutant *eif4g eif4e1*, known as *eif4f* (Patrick and Browning, 2012), and that of the two redundant eIFiso4G genes, *eifiso4g1 eifiso4g2*, (Lellis et al., 2010) for translation of R-motif-containing dual luciferase reporters made from the R-motif-containing 5′ leader sequences of *TBF1*, *ZIK3*, and *ATG8E*. We found that without PTI signaling, translation of these reporters was increased in the *eif4g eif4e1* mutant but decreased in the *eifiso4g1 eifiso4g2* mutant compared with WT (Figures S3H and S3I), suggesting that eIF4G and eIFiso4G may be negative and positive regulators of R-motif-mediated translation, respectively. Noticeably, for the control mRNA without an R-motif, translation was decreased in the *eif4g eif4e1* mutant (Figure S3H), consistent with eIF4G and eIF4E being canonical translation initiation factors, but not in the *eifiso4g1 eifiso4g2* mutant (Figure S3I), supporting eIFiso4G's specific activity in R-motif-dependent translation. Also, consistent with their proposed opposing roles in PTI-specific translation, the *eif4g eif4e1* mutant displayed either WT or higher-than-WT level of elf18-induced reporter activities (Figure 3C), whereas the *eifiso4g1 eifiso4g2* mutant failed to respond to the induction (Figure 3D).

## PABPs regulate basal resistance and PTI through eIF4G and eIFiso4G, respectively

To determine whether translational perturbations observed in the mutants of PABP, eIF4G, and eIFiso4G impact basal and elf18-triggered immunity, we inoculated the mutants with *Pseudomonas syringae* pathovar *maculicola* (*Psm*) ES4326. We found the *pab2.5* mutant to have significantly enhanced basal resistance to *Psm* ES4326 but compromised elf18-induced resistance to the pathogen (Figure 4A), consistent with our previous report using lower order mutants (Xu et al., 2017). In the *eif4g* and *eif4g eif4e1* mutants, higher-than-WT levels of basal resistance (Figure 4B), but normal elf18-triggered protection, were observed. In contrast, the *eifiso4g1 eifiso4g2* mutant was only compromised in elf18-induced resistance to *Psm* ES4326, with normal basal resistance (Figure 4C). Interestingly, mutants of the cap-binding proteins eIF4E and eIFiso4E had no effect on elf18-induced resistance against *Psm* ES4326 (Figures 4B and 4C), supporting our hypothesis that these cap-binding proteins are dispensable for PTI.

The relationship between PABP and eIF4G or eIFiso4G in regulation of basal and elf18-triggered immunity was then studied using quadruple mutants *pab2 pab8 eif4g eif4e1* and *pab2 pab4 eifiso4g1 eifiso4g2*. The *pab2 pab4 eifiso4g1 eifiso4g2* mutant was used instead of *pab2 pab8 eifiso4g1 eifiso4g2* because the latter was not viable in our growth conditions. We found the *pab2 pab8 eif4g eif4e1* mutant to have similarly enhanced basal defense to *Psm* ES4326 as the *eif4g eif4e1* double mutant (Figure 4D), consistent with our hypothesis that the canonical eIF4G/4E1 work downstream of PABP to inhibit basal resistance. In contrast, mutating eIFiso4G in the *pab2 pab4 eifiso4g1 eifiso4g2* quadruple mutant not only reduced basal resistance to the WT level but also compromised elf18-induced defense (Figure 4E), demonstrating that eIFiso4G, in association with PABP, plays a positive role in conferring basal resistance as well as in inducing PTI.

## MPK3/6 phosphorylate PABP to enhance its binding to R-motif and promote plant immunity

To elucidate the signal pathway that leads to the switch from canonical cap-dependent translation to PABP/R-motif-mediated cap-independent translation upon pathogen perception, we focused on the second ''hub protein,'' RACK1A, identified in our LC-MS/MS analysis (Figure 3A; Table S3). RACK1 is a noteworthy PABP interactor because its knockdown mutant has a defense phenotype similar to that of *pab2.5* (Figure 4F), and it physically and genetically interacts with PABPs, eIF4G, and eIFiso4G (Figure S4). More importantly, RACK1 is not only a 40S ribosome-associated protein (Ceci et al., 2003; Sengupta et al., 2004) but also known as a scaffold that bridges MPK3/6 with the heterotrimeric G-protein complex during PTI (Cheng et al., 2015). Since MPK3/6 are essential regulators of PTI-associated transcription, we tested the possibility that MPK3/6 have an additional function in directing translational reprogramming early in this immune response by transforming the R-motif-containing dual luciferase reporters into the inducible *mpk3 mpk6* double-mutant (*mpk6SR*) protoplasts. We found that knocking down the MPK3/6 function indeed compromised elf18-induced translation of the *TBF1*, *ZIK3*, and *ATG8E* reporters (Figures S5A–S5C).

To test whether MPK3/6 regulate R-motif-containing mRNA translation by phosphorylating R-motif-associated translation regulators, we first performed the phos-tag gel analysis on the PAB8 protein expressed in *Arabidopsis* protoplasts after elf18 treatment and found an elf18-induced transient mobility shift of the protein (Figure 5A) which is sensitive to phosphatase treatment (Figure S5D). We next treated the transgenic lines expressing PAB2, PAB4, and PAB8 with elf18 to further confirm the results *in planta*. Surprisingly, we found that this elf18-triggered mobility shift was only observed in PAB8 (Figure S5E), not in PAB2 or PAB4 (Figure S5F). It is worth noting that the timing of PAB8

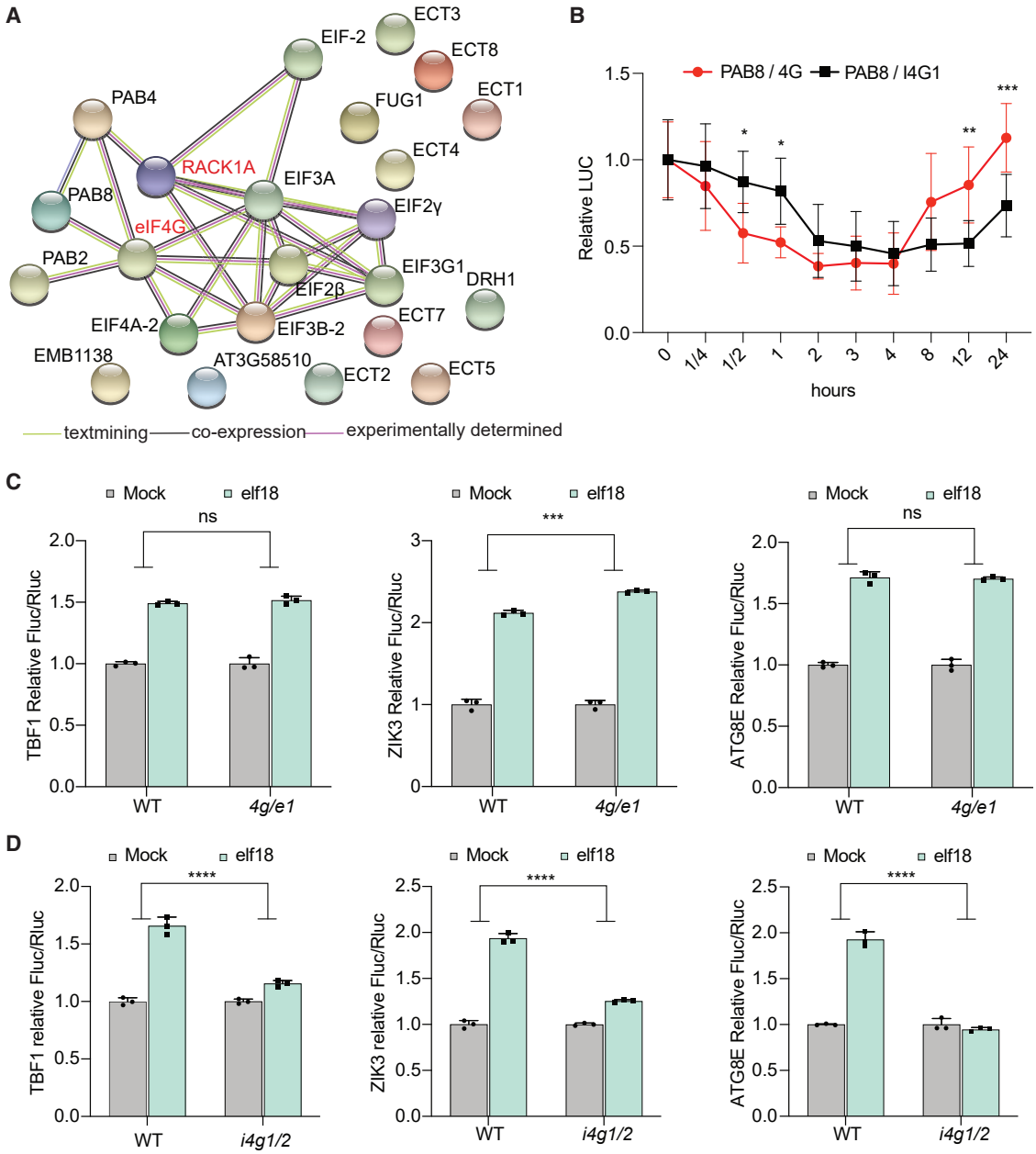


**Figure 3. PABPs regulate R-motif-containing defense mRNA translation through differential association with eIF4G and eIFiso4G**

(A) STRING analysis of PABP-interacting proteins identified using LC-MS/MS (related to Table S3) . Text-mining, coexpression, and experiments were chosen as active interaction sources, interaction score = 0.700.

(B) The dynamics of the interaction between PAB8 and eIF4G (4G) or eIFiso4G1 (I4G1) upon elf18 treatment were determined using the split-luciferase assay in which Cluc-tagged PAB8 and Nluc-tagged eIF4G (4G) or eIFiso4G1 (I4G1) were transiently coexpressed in *Nb* plants for 2 days. Data are values (elf18/mock) normalized to time zero.

(C and D) Elf18-induced translation of R-motif-containing mRNAs, *TBF1*, *ZIK3*, and *ATG8E*, was measured using *TBF1*, *ZIK3*, and *ATG8E* 5′ leader sequences in dual luciferase reporters after overnight expression in protoplasts made from WT, *eif4g eif4e1* (*4g/e1*) (C), and *eifiso4g1 eifiso4g2* (*i4g1/2*) (D) plants. The resulting protoplasts were treated with 1 μM elf18 for 45 min before luciferase activities were measured. Values are means ± SDs.

Each dot represents a biological replicate. Data were analyzed via two-way ANOVA with Dunnett multiple comparisons (B) and two-way ANOVA (C and D), *p < 0.05, **p < 0.01, ***p < 0.001, ****p < 0.0001. ns, not significant. See also Figure S3.

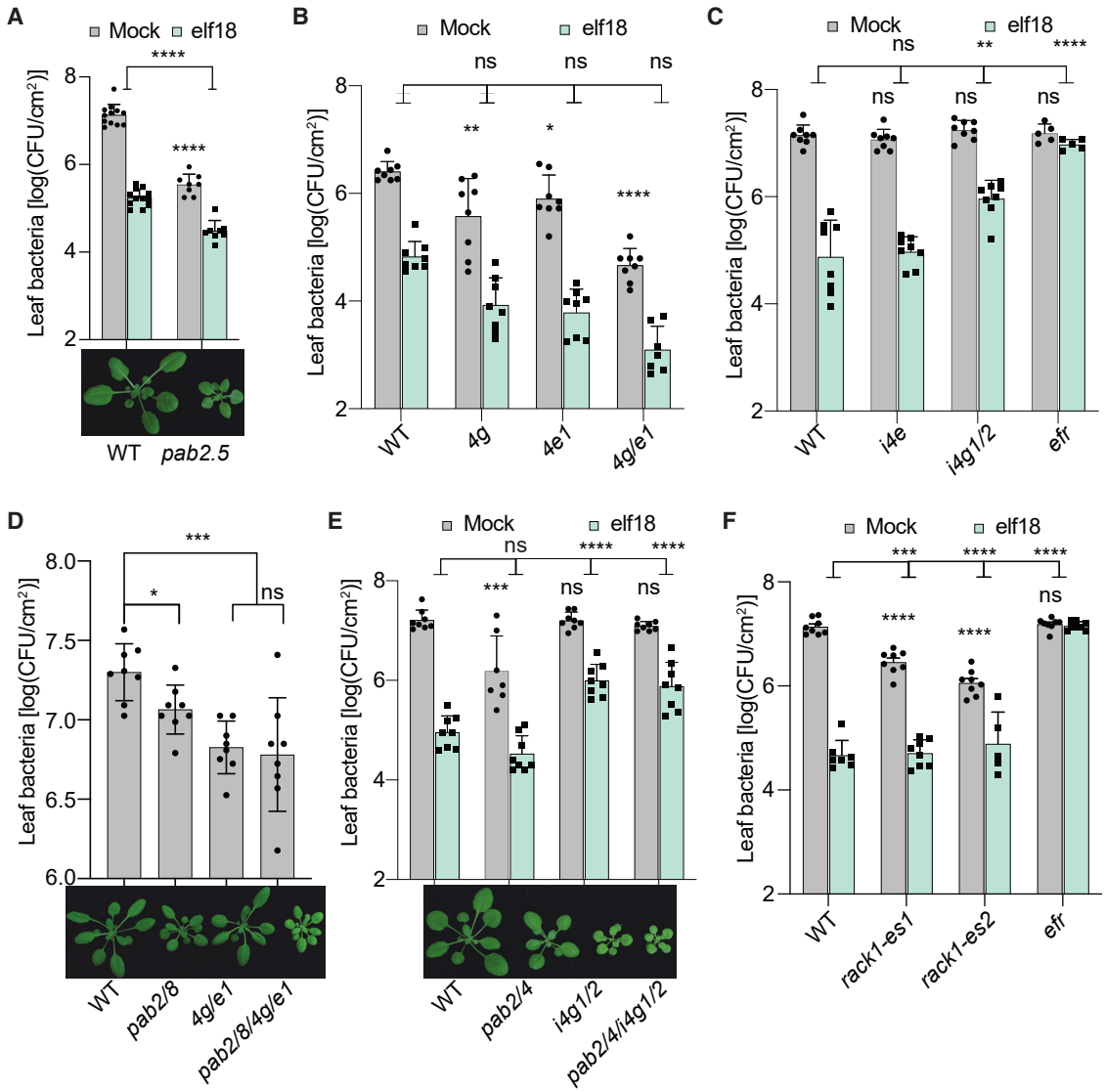


**Figure 4. PABP and RACK1 regulate basal resistance and PTI through eIF4G and eIFiso4G**

(A–C) Elf18-induced resistance. 4-week-old *Arabidopsis* plants were infiltrated with *Psm* ES4326 ($OD_{600nm}$ = 0.001) 24 h after 1 μM elf18 or water treatment, and bacterial growth was assessed 2 days later in the mutants of PABP (A), eIF4G and 4E1 (B), eIFiso4G1, and eIFiso4G2 (C). *pab2.5*, *pab2 pab8 pab4*$^{+/-}$; *4g*, *eif4g*; *4e1*, *eif4e1*; *4g/e1*, *eif4g eif4e1*; *i4g1*, *eifiso4g1*; *i4g2*, *eifiso4g2*; *i4g1/2*, *eifiso4g1 eifiso4g2; efr*, the elf18 receptor mutant.

(D) Basal resistance. Bacterial infection was performed as in (A)–(C) without the elf18 pre-treatment. *pab2/8*, *pab2 pab8*; *pab2/8/4g/e1*, *pab2 pab8 eif4g eif4e1*.

(E and F) Elf18-induced resistance. Bacterial infection was performed as in (A)–(C) in the *pab2/4/i4g1/2* mutant (E) and the estradiol-inducible (50 μM estradiol) *RACK1* knockdown mutant lines *rack1-es1* and *rack1-es2* (F). *pab2/4/i4g1/2*, *pab2 pab4 eifiso4g1 eifiso4g2*.

Photos of plants were taken before infection (A, D, and E). Values are means of log colony-forming units per leaf area (CFU/cm$^2$) ± SDs. Each dot represents a biological replicate. Data were analyzed by t test (D) and two-way ANOVA (A–C, E, and F), *p < 0.05, **p < 0.01, ***p < 0.001, ****p < 0.0001. ns, not significant. See also Figure S4.

phosphorylation (Figure 5A) coincided well with its enhanced association with R-motif (Figure 2E), suggesting that PAB8 binding to R-motif is modulated by its phosphorylation status.

To identify the phosphorylation site(s) in PAB8, we conducted LC-MS/MS analysis and detected only one elf18-induced phosphorylation residue, S566 (Figure S5G), and this residue is absent in PAB2 and PAB4, indicating that if phosphorylation does occur in these proteins, it is likely to be at different residues and not detectable by the phos-tag gel (Figure S5F). Site-directed mutagenesis was performed to substitute S566 with alanine and the PAB8$^{S566A}$ mutation completely abolished the elf18-induced mobility shift of the PAB8 protein (Figure 5B). Interestingly, this serine is in a typical MPK3/6 phosphorylation motif X-(Ser/Thr)-Pro (Clark-Lewis et al., 1991; Sörensson et al., 2012), consistent with our hypothesis that MPK3/6 are the kinases regulating PABP activities during PTI.

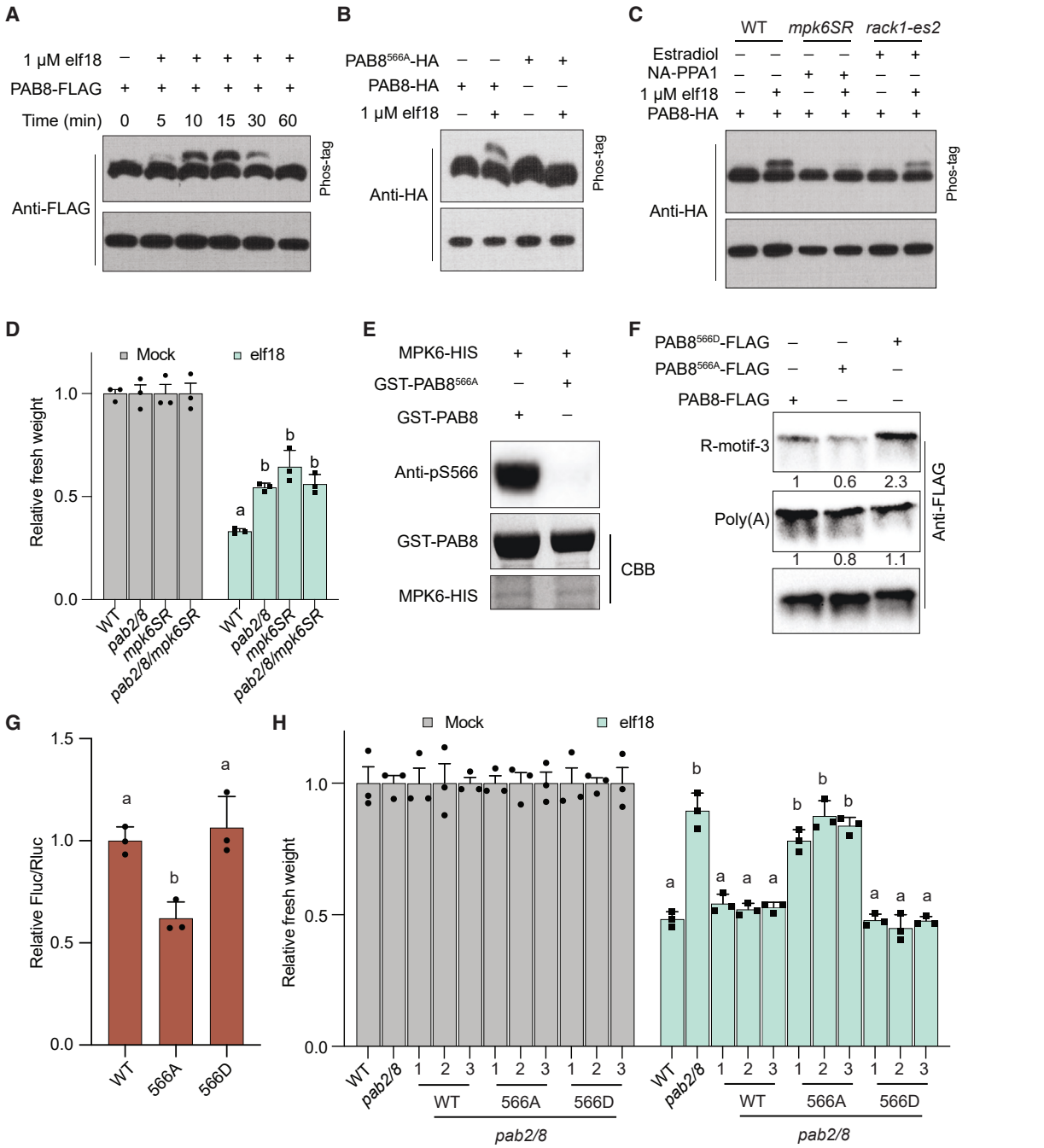


**Figure 5. MPK3/6 phosphorylate PABP during PTI to enhance its binding to R-motif**

(A) Elf18-induced PAB8 protein mobility shift. PAB8-FLAG was extracted from protoplasts after treatment with 1 μM elf18 for the indicated time. Protein mobility was analyzed using a phos-tag gel immunoblotted with an anti-FLAG antibody.

(B) Ser566 as the phospho-site in PAB8. PAB8-HA or the PAB8$^{S566A}$-HA mutant protein was produced and analyzed as in (A) with an anti-HA antibody.

(C) Elf18-induced phosphorylation of PAB8 by MPK3/6. PAB8-HA was expressed in WT, *mpk6SR* (inhibitor-sensitized MPK3 variant-rescued *mpk3 mpk6* double mutant), and *rack1-es2* protoplasts in the presence of 2-μM NA-PP1 inhibitor (*mpk6SR*) and 50 μM estradiol (*rack1-es2*), respectively, and analyzed as in (A) with an anti-HA antibody.

(D) Elf18-associated growth inhibition. 5-day-old seedlings were pre-treated with or without 2-μM NA-PP1 overnight, followed by water or 100 nM elf18 treatment for 3–4 days before fresh weight was measured. *pab2/8*, *pab2 pab8*. Values are means ± SEMs.

(E) *In vitro* PAB8$^{S566}$ phosphorylation by MPK6. Protein phosphorylation was detected by anti-pS566 antibodies. CBB, Coomassie Brilliant Blue G-250.

*(legend continued on next page)*

To test this hypothesis, we first confirmed the MPK3/6-PAB8 interaction (Figure S5H) and then examined the elf18-induced PAB8 band shift in the *mpk6SR* mutant and the kinase scaffold RACK1 knockdown mutant *rack1-es2* and found the band shift diminished in each mutant (Figure 5C). To further confirm that MPK3/6 work with PABP in the same pathway, we crossed *pab2 pab8* with *mpk6SR* and found the resulting *pab2 pab8 mpk6SR* line similarly compromised in response to elf18-associated plant growth inhibition as the parents (Figure 5D). Moreover, in an *in vitro* phosphorylation assay, MPK6 was shown to phosphorylate PAB8, but not the PAB8$^{S566A}$ variant, using a phospho-specific antibody against pSer566 (Figure 5E). These data clearly demonstrate that MPK3/6 phosphorylate PAB8 at Ser566 during elf18-triggered PTI.

To determine whether this modification is responsible for the enhanced PAB8 binding to R-motifs (Figure 2E), we performed R-motif binding assay using proteins produced in protoplasts. Immunoblotting analysis showed that the phosphodead PAB8$^{S566A}$ had a weakened binding to R-motif 3, whereas the phosphomimetic PAB8$^{S566D}$ had a stronger binding (Figure 5F), confirming that the dynamic change in PABP association with R-motif is indeed regulated through its phosphorylation. Using RNA-immunoprecipitation-qPCR, we further showed that *in planta*, PAB8$^{S566D}$ had a significantly higher level of association with R-motifs in the *TBF1* 5′ leader sequence than PAB8$^{S566A}$ (Figure S5I).

To examine whether PAB8$^{S566}$ phosphorylation affects its function in translation, we coexpressed PAB8, PAB8$^{S566A}$, and PAB8$^{S566D}$ with the *TBF1* dual luciferase reporter *35S:uORF/R$_{TBF1}$-FLUC/35S:RLUC* in *Nb* plants. The results showed that PAB8$^{S566A}$ had a much lower reporter translation than the WT PAB8 and PAB8$^{S566D}$ (Figure 5G). The role of PAB8$^{S566}$ phosphorylation in PTI response was then examined by introducing *PAB8*, *PAB8$^{S566A}$*, or *PAB8$^{S566D}$* transgenes under the control of its native promoter (NP) into the *pab2 pab8* mutant. Although introduction of the *NP:PAB8-HA* or *NP:PAB8$^{S566D}$-HA* transgene restored plants sensitivity to elf18-induced growth retardation, the *NP:PAB8$^{S566A}$-HA* transgene failed to do so (Figure 5H). The fact that the *NP:PAB8$^{S566D}$-HA/pab2 pab8* plants are responsive to elf18 induction indicates that phosphorylation of PAB8 is necessary but not sufficient for PTI induction.

## MPK3/6 phosphorylate eIF4G and eIFiso4G to inhibit general translation while activating defense mRNA translation

Besides PABPs, we also considered the associated eIF4G and eIFiso4G as potential substrates of MPK3/6. We first detected an elf18-specific and phosphatase-sensitive band shift of eIF4G which occurred as early as 5 min post treatment (Figures 6A and S6A). Through LC-MS/MS analysis, we identified fifteen phosphorylation sites in eIF4G with eight of them having a typical MPK3/6 phosphorylation motif (Figure S6B, highlight in red) (Clark-Lewis et al., 1991; Sörensson et al., 2012). Because eIF4G is nearly 190 kDa in MW and poorly resolved on a phos-tag gel (Figures 6A and S6A), we truncated eIF4G into the N-terminal (4G-N) and the C-terminal (4G-C) halves, respectively, and performed simultaneous alanine substitutions. The resulting mutants significantly reduced the elf18-induced band shift, with mutants of those eight MPK3/6 phosphorylation residues Ser530, Ser1066, Thr1069, Ser1366, Ser1367, Ser1376, Ser1508, and Ser1527 showing the most significant effects (“3A” in Figure S6C and “5A” in Figure S6D), indicating that they are major phosphorylation sites in eIF4G responsive to elf18 treatment through the activity of MPK3/6.

The dependency on MPK3/6 was confirmed by demonstrating that MPK3/6 interact with eIF4G (Figures S6E and S6F) and by *in planta* testing using the *mpk6SR* mutant in which the elf18-induced band shift was significantly diminished in the mutant (Figure S6G). We next demonstrated that MPK6 could phosphorylate eIF4G directly using an *in vitro* kinase assay followed by immunoblotting using antibodies against phospho-eIF4G$^{S1066,T1069}$ (pSer1066/Thr1069) (Figure 6B). To examine the impact of MPK3/6-mediated phosphorylation on eIF4G translational activity, we transiently expressed mutants of all eight MPK3/6 target sites eIF4G$^{8A}$ or eIF4G$^{8D}$ with the *TBF1* dual luciferase reporter in *Nb* plants. We found that the phosphodead eIF4G$^{8A}$ mutant supported higher-than-WT reporter translation, whereas the phosphomimetic eIF4G$^{8D}$ mutant had little effect (Figure 6C), indicating that phosphorylation of eIF4G negatively impacts translation of the reporter either through reduced activity or dissociation from PABPs. Therefore, MPK3/6-mediated phosphorylation of eIF4G is another mechanism, beside decapping of mRNA, for plants to rapidly inhibit canonical translation in response to pathogen challenge.

We next examined the phosphorylation of eIFiso4G1 and found that similar to PAB8 and eIF4G, there were phosphorylation-associated band shifts in the protein following elf18 perception, which occurred within 5 min of treatment (Figures 6D and S6H). Using LC-MS/MS analysis, we identified two phosphorylation sites, S487 and S542, in eIFiso4G1, both within the typical MPK3/6 phosphorylation motif (Figure S6I). Interestingly, S542 phosphorylation by Snf1-related protein kinase 1 was also observed during hypoxia (Cho et al., 2019). Simultaneously substituting these two residues with alanine

(F) The interaction between R-motif and PAB8 phosphorylation variants. FLAG-tagged PAB8 and phospho-site variants purified from protoplasts and pulled down by *TBF1* R-motif 3 were quantified by immunoblotting using an anti-FLAG antibody. Numbers under each blot are the ratios to PAB8-FLAG normalized to the input (bottom blot).

(G) The effect of PAB8$^{S566}$ phosphorylation on translation. The *TBF1* dual luciferase reporter translational activity was determined 2 days after transient coexpression with PAB8-HA (WT), PAB8$^{S566A}$-HA (566A), or PAB8$^{S556D}$-HA (566D) in *Nb* plants. Values are means ± SDs.

(H) Elf18-associated growth inhibition. 5-day-old independent *Arabidopsis* transgenic lines (in *pab2 pab8*) expressing *NP:PAB8-HA* (WT), *NP:PAB8$^{S556A}$-HA* (556A), or *NP:PAB8$^{S556D}$-HA* (556D) were treated with mock or 100 nM elf18 for 3–4 days before fresh weight was measured. *NP*, PAB8 native promoter. Values are means ± SDs.

Each dot represents a biological replicate. Data were analyzed by one-way ANOVA (Tukey) (G) and two-way ANOVA with Dunnett multiple comparisons (D and H), different letters indicate statistical significance, $p < 0.05$. See also Figure S5.

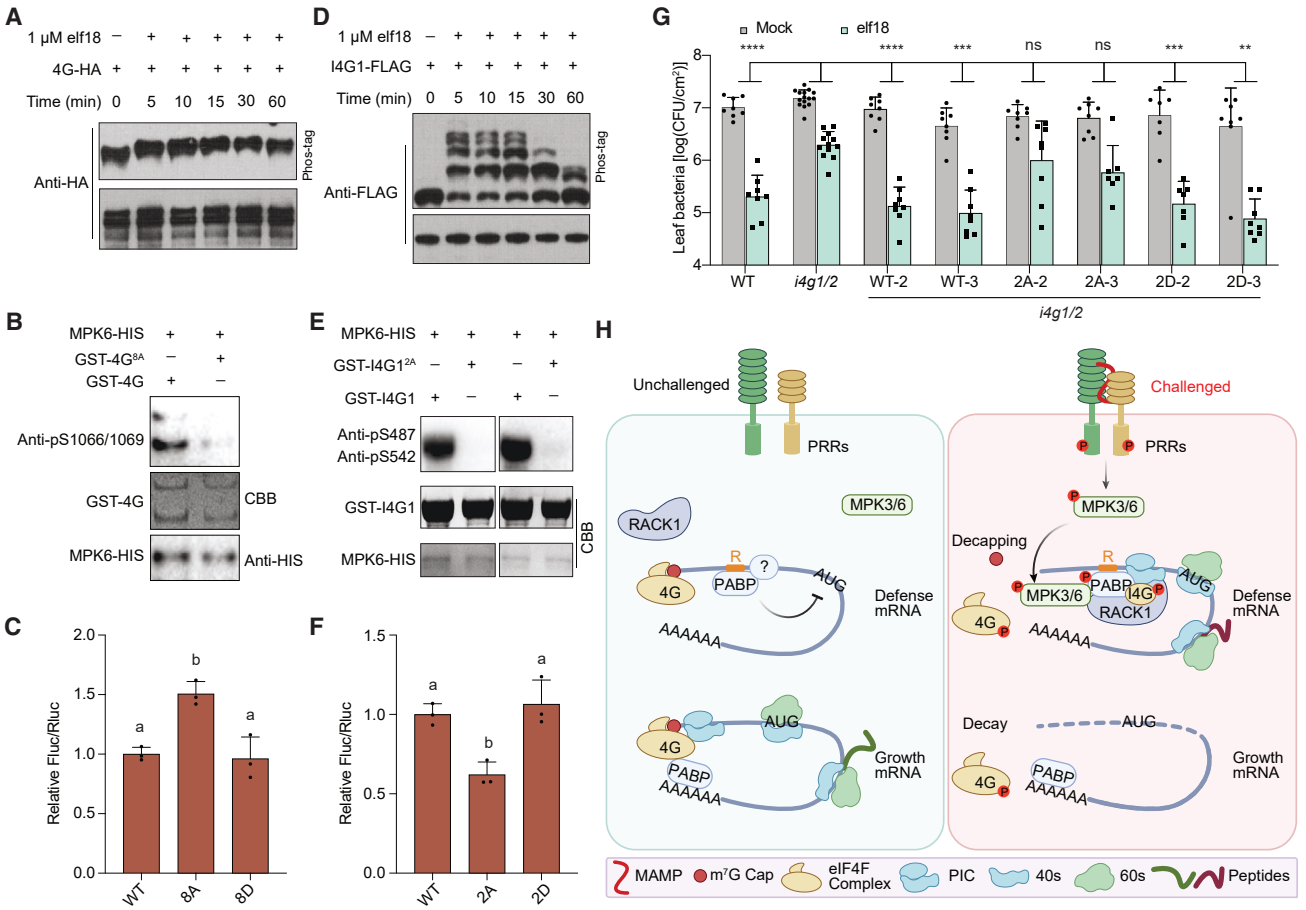


**Figure 6. MPK3/6-mediated phosphorylation inhibits eIF4G while activating eIFiso4G to reprogram translation during PTI**

(A) Elf18-induced eIF4G protein mobility shift. eIF4G-HA (4G-HA) was extracted from protoplasts after treatment with 1 μM elf18 for the indicated time. Mobility change of the protein was examined using a phos-tag gel immunoblotted with an anti-HA antibody.

(B) *In vitro* eIF4G$^{S1066/T1069}$ phosphorylation by MPK6. Protein phosphorylation was detected by anti-pS1066/T1069 antibodies. GST-eIF4G, GST-4G; GST-4G$^{8A}$, alanine mutant of the eight MPK3/6 target sites. CBB, Coomassie Brilliant Blue G-250.

(C) The effect of eIF4G phosphorylation on translation. The *TBF1* dual luciferase reporter translational activity was determined 2 days after transient coexpression with eIF4G-HA (WT), eIF4G$^{8A}$ (8A), or eIF4G$^{8D}$ (8D) in *Nb* plants. 8D, aspartic acid mutant of the eight MPK3/6 target sites. Values are means ± SDs.

(D) Elf18-induced eIFiso4G1 protein mobility shift. eIFiso4G1-FLAG (I4G1-FLAG) was extracted from protoplasts after treatment with 1 μM elf18 for the indicated time. Mobility change of the protein was examined using a phos-tag gel immunoblotted with an anti-FLAG antibody.

(E) *In vitro* eIFiso4G1$^{S487/S542}$ phosphorylation by MPK6. Protein phosphorylation was detected by anti-pSer487 antibodies (left) and anti-pSer542 antibodies (right). GST-eIFiso4G1, GST-I4G1; GST-eIFiso4G1$^{S487A/S542A}$, GST-I4G1$^{2A}$. CBB, Coomassie Brilliant Blue G-250.

(F) The effect of eIFiso4G phosphorylation on translation. The *TBF1* dual luciferase reporter translational activity was determined 2 days after transient coexpression with eIFiso4G-HA (WT), eIFiso4G1$^{S487A/S542A}$ (2A), or eIF4isoG1$^{S487D/S542D}$ (2D) in *Nb* plants. Values are means ± SDs.

(G) Elf18-induced resistance. 4-week-old independent *Arabidopsis* transgenic lines in *eifiso4g1 eifiso4g2* (*i4g1/2*) expressing *NP:eIFiso4G1-HA* (WT), *NP:eIFiso4G1$^{S487A/S542A}$-HA* (2A), or *NP:eIFiso4G1$^{S487D/S542D}$-HA* (2D) were infiltrated with *Psm* ES4326 ($OD_{600nm}$ = 0.001) 24 h after 1 μM elf18 or water treatment, and bacterial growth was assessed 2 days later. *NP*, eIFiso4G1 native promoter. Values are means ± SDs

(H) PABP/R-motif-mediated cap-independent translation reprogramming upon PTI induction. In the absence of pathogen challenge, growth mRNAs are translated through the canonical cap-dependent mechanism, whereas for defense mRNAs with an R-motif (R), translation is inhibited by PABP through an unknown mechanism (?). Upon perception of pathogen challenge by PRRs, MPK3/6 are activated to induce mRNA decapping and repress eIF4G activity by phosphorylation to inhibit translation of growth mRNAs. For defense mRNAs carrying an R-motif, translation is initiated using R-motif as an IRES through PABP-mediated recruitment of eIFiso4G after phosphorylation by MPK3/6 on the scaffold protein RACK1.

Each dot represents a biological replicate. Data were analyzed by one-way ANOVA (Tukey) (C and F) and two-way ANOVA (G), different letters indicate statistical significance, $p < 0.05$; $^{**}p < 0.01$, $^{***}p < 0.001$, $^{****}p < 0.0001$. ns, not significant. See also Figure S6.

significantly decreased elf18-induced band shift (Figure S6J). The role of MPK3/6 in phosphorylating eIFiso4G1 was then demonstrated *in planta* based on the MPK3/6-eIFiso4G interaction data (Figure S6K) as well as the phos-tag gel analysis using the *mpk6SR* and *rack1-es2* mutants (Figure S6L). We then performed *in vitro* phosphorylation reaction on eIFiso4G1 followed by immunoblotting analysis using antibodies against phospho-Ser487 (pSer487) and phospho-Ser542 (pSer542) in the protein

and found MPK6 could phosphorylate eIFiso4G1 directly (Figure 6E).

The effect of phosphorylation on eIFiso4G translational activity was examined by coexpressing different eIFiso4G1 variants with the *TBF1* dual luciferase reporter in *Nb* plants. Opposite to the canonical eIF4G (Figure 6C), the phosphodead eIFiso4G1$^{2A}$ mutant had significantly less, whereas the phosphomimetic eIFiso4G1$^{2D}$ mutant had a similar reporter translation compared with the WT eIFiso4G1 (Figure 6F), indicating that MPK3/6-mediated phosphorylation enhances translational activity of eIFiso4G. Subsequent genetic complementation experiment using *NP:eIFiso4G1*, *NP:eIFiso4G1$^{2A}$*, and *NP:eIFiso4G1$^{2D}$* showed that introducing either the *eIFiso4G1* or *eIFisoI4G1$^{2D}$* transgene restored PTI-induced growth inhibition to the *eifiso4g1 eifiso4g2* mutant (Figure S6M). In contrast, independent transformants with the *NP:eIFiso4G$^{2A}$* transgene completely failed to restore the elf18-associated growth inhibition. Finally, we tested PTI-associated resistance on the transgenic lines and observed that similar to elf18-induced growth inhibition results (Figure S6M), *NP:eIFiso4G1* and *NP:eIFiso4G1$^{2D}$*, but not *NP:eIFiso4G1$^{2A}$*, rescued the PTI-deficient phenotype of the *eifiso4g1 eifiso4g2* mutant (Figure 6G). Together, these data demonstrate that through MPK3/6-mediated phosphorylation of PABP, eIF4G, and eIFiso4G, plants can quickly reprogram their translatome upon pathogen perception.

## DISCUSSION

This study demonstrates that in response to immune induction, R-motif serves as a cellular IRES to mediate cap-independent stress protein translation (Figure 6H). Normally, translation from R-motif is repressed either through cap-mediated competition for PABPs via the poly(A) tail or by an unknown inhibitor associated with PABPs. Upon immune induction, there is an increase in mRNA decapping activity, relieving cap-competition with PABP/R-motif-mediated translation. However, whether decapping is required for this alternative translation mechanism needs further investigation. Another question that remains to be answered is: does R-motif-mediated translation occur in the P-bodies where decapping is known to occur or are decapped mRNAs released into the cytosol for translation? The previous report of transient disappearance and reappearance of P-bodies after PTI induction (Yu et al., 2019) suggests that the latter is a plausible hypothesis. Alternatively, decapping-mediated mRNA decay and activation of PABP/R-motif-mediated translation of defense mRNAs may be two separate events in PTI induction.

In plants, both eIF4G and eIFiso4G can initiate protein translation under normal growth conditions. As a plant-specific isomer, eIFiso4G has been reported to also translate mRNAs under certain stress conditions, such as hypoxia and viral infection, through an unknown mechanism (Cho et al., 2019; Nicaise et al., 2007). It is interesting to note that the *eif4f* plants (i.e., the *eif4g eif4e1* double mutant) are morphologically similar to WT (Figure 4D), probably due to compensatory expression of eIFiso4G (Bi et al., 2019). Upregulation of eIFiso4G may also explain the high basal resistance observed in the *eif4f* mutant (Figures 4B and 4D). In contrast to *eif4f*, the *eifiso4g1 eifiso4g2* mutant plants have a reduced stature (Figure 4E; Bi et al., 2019), implying that a deficiency in eIFiso4G cannot be reciprocally compensated by eIF4G. The differential dissociation and reassociation of eIF4G and eIFiso4G from PABPs following elf18 induction (Figures 3B, S3F, and S3G) show that during PTI, distinct eIFs are dynamically recruited by PABPs to the R-motif and/or the 5′ cap, depending on the mRNA sequence and structure, to translate defense mRNAs.

This study also found that the immune-induced translational reprogramming is mediated by the essential PTI regulators MPK3/6, previously known mainly for their role in regulating transcription (Bigeard et al., 2015; Meng and Zhang, 2013; Rasmussen et al., 2012). Upon immune induction, MPK3/6 turn off the canonical cap-dependent translation through induction of mRNA decapping (Figures 1 and S1; Xu and Chua, 2012; Yu et al., 2019) and inhibition of eIF4G activity, while turning on the R-motif-dependent translation through enhancement of the "PABP/R-motif" translation initiation module (Figures 5 and 6). A previous study showed that eIF4G's translational activity could also be inhibited by phosphorylation upon photosynthetic input (Boex-Fontvieille et al., 2013), indicating that this key translation initiation factor is regulated by different environmental stresses. Consistent with this hypothesis, we found 15 phosphorylation events in eIF4G (Figure S6B), and 8 of them are modified by MPK3/6. Whether different environmental stresses inhibit eIF4G through the same phosphorylation sites or different ones need to be further studied.

The rapidity of the phosphorylation events suggests that the MPK3/6-controlled translational reprogramming is an initial event in PTI induction. Consistent with this hypothesis, knocking down MPK3/6 (*mpk6SR*) in the *pab2 pab8* mutant did not further compromise the responsiveness of the higher order mutant to elf18 (Figure 5D). It is likely that defense transcription factors, such as TBF1, must be translated from preexisting mRNAs to trigger transcriptional reprogramming. It is also worth noting that R-motifs have been found in the 5′ leader sequences of *MPK6*, *PAB2*, *PAB4*, *PAB8*, *eIFiso4G1*, and *eIFiso4G2*, but not that of *eIF4G* (Xu et al., 2017), suggesting that these regulators of PTI-associated translation can also be produced through R-motif-mediated translation, forming an amplification loop.

It will be interesting to determine whether this cap-independent PABP/R-motif translational module functions in stress responses of other higher eukaryotes. In yeast, cap-independent translation of several mRNAs involved in invasive growth has been found to require Pab1p binding to a poly(A) stretch in their 5′ UTRs (Gilbert et al., 2007). Our previous study showed that R-motif is prevalent in the 5′ leader sequences of stress mRNAs from *Drosophila*, mouse to human, including the human p53 mRNA (Xu et al., 2017). Translation of these mRNAs may be similarly switched on in response to stress by phosphorylation of PABP and translation initiation factors.

### Limitations of the study

The limitations of the study are intrinsic to the translation process, which is impacted by a myriad of factors at different levels of regulation. Since plants do not have specialized immune cells,

perturbation of plant defense-related translational activity is likely to also influence plant growth and development. To overcome these challenges, we had to use proxies to deduce the PTI-specific translational effects in a few experiments. For example, PTI-induced growth inhibition of plate-grown seedlings, a phenotype that is certain to result in part from immune-induced translatome reprogramming, is used to minimize environmental variations and obtain reproducible quantitative data in characterizing the translation mutants. As shown in Figure S6M, the PTI-induced growth inhibition assay results are consistent with the observed PTI-associated resistance (Figure 6G). Another challenge for the study is the involvement of essential genes, such as *DCP2*, *PABPs*, *RACK1*, and *MPK3/6*. For example, *PABPs* are required for both growth- and defense-related translation, and there are eight *PABPs* in the *Arabidopsis* genome. Higher order *pab* mutants are required to observe a defense phenotype, which is also influenced by the plant growth conditions. Among the three PABPs tested, only PAB8 had a detectable elf18-induced mobility shift on a phos-tag gel, leaving the phosphorylation status of other PABPs unknown. Finally, this study focuses on elucidating the role of R-motif in PTI-mediated translation. However, besides the R-motif, defense mRNAs contain other regulatory elements in their 5′ leader sequences, such as the two uORFs found downstream of R-motif 1 and R-motif 2, respectively, in the *TBF1* mRNA. Nevertheless, the elucidation of the role of R-motif as a cellular IRES and the establishment of the signaling pathway linking pathogen perception to R-motif-mediated translation activation in this study provide a necessary framework for future research.

## STAR★METHODS

Detailed methods are provided in the online version of this paper and include the following:

- KEY RESOURCES TABLE
- RESOURCE AVAILABILITY
  - Lead contact
  - Materials availability
  - Data and code availability
- EXPERIMENTAL MODEL AND SUBJECT DETAILS
- METHOD DETAILS
  - Plasmid construction
  - Confocal laser scanning microscopy
  - Decapping assay, RNA isolation and qPCR
  - Elf18-induced growth inhibition assay
  - Luciferase reporter assay
  - *In vitro* translation assay in wheat-germ system
  - PABP/R-motif binding assay
  - LC-MS/MS analysis
  - STRING analysis
  - Split-luciferase assay and co-IP assay
  - Elf18-induced infection protection assay
  - Phos-tag gel assay
  - Antibody preparation
  - *In vitro* phosphorylation assay
  - RNA-immunoprecipitation qPCR assay
- QUANTIFICATION AND STATISTICAL ANALYSIS

## SUPPLEMENTAL INFORMATION

Supplemental information can be found online at https://doi.org/10.1016/j.cell.2022.06.037.

## ACKNOWLEDGMENTS

We thank Dr. Karen Browning for sharing the *eif4g*, *eif4g eif4e1*, and *eifiso4g1 eifiso4g2* mutants and for helpful input to the manuscript; Dr. Fred Ausubel for providing the *rack1-es1* and *rack1-es2* transgenic lines; Dr. Maria Barna for sharing the Hoxa3 TIE sequence; and members of the Dong lab for discussion and critical reading of the manuscript. This work was supported by grants from the National Science Foundation (IOS-1645589 and IOS-2041378), National Institutes of Health (R35-GM118036-06), and the Howard Hughes Medical Institute to X.D.

## AUTHOR CONTRIBUTIONS

J.W. and X.D. designed the study. J.W. performed most of the experiments. X.Z. helped with the P-body imaging. G.H.G. provided R-motif analysis of the *TBF1* mRNA. G.X. helped with plasmid construction and the dual luciferase assay. J.W., X.Z., G.H.G., and X.D. wrote the paper.

## DECLARATION OF INTERESTS

X.D. is a founder of Upstream Biotechnology Inc. and a member of its scientific advisory board, as well as a scientific advisory board member of Inari Agriculture Inc. G.H.G. is a founder of Upstream Biotechnology Inc. Claims protecting IP rights to purine-rich elements are pending in U.S. patent publication US2019-0352664.

Received: October 20, 2021
Revised: May 3, 2022
Accepted: June 21, 2022
Published: July 27, 2022

## REFERENCES

Bertrand, E., Chartrand, P., Schaefer, M., Shenoy, S.M., Singer, R.H., and Long, R.M. (1998). Localization of ASH1 mRNA particles in living yeast. Mol. Cell *2*, 437–445.

Bi, C., Ma, Y., Jiang, S.C., Mei, C., Wang, X.F., and Zhang, D.P. (2019). *Arabidopsis* translation initiation factors eIFiso4G1/2 link repression of mRNA cap-binding complex eIFiso4F assembly with RNA-binding protein SOAR1-mediated ABA signaling. New Phytol. *223*, 1388–1406.

Bi, G., Zhou, Z., Wang, W., Li, L., Rao, S., Wu, Y., Zhang, X., Menke, F.L.H., Chen, S., and Zhou, J.-M. (2018). Receptor-like cytoplasmic kinases directly link diverse pattern recognition receptors to the activation of mitogen-activated protein kinase cascades in *Arabidopsis*. Plant Cell *30*, 1543–1561.

Bigeard, J., Colcombet, J., and Hirt, H. (2015). Signaling mechanisms in pattern-triggered immunity (PTI). Mol. Plant *8*, 521–539.

Boex-Fontvieille, E., Daventure, M., Jossier, M., Zivy, M., Hodges, M., and Tcherkez, G. (2013). Photosynthetic control of *Arabidopsis* leaf cytoplasmic translation initiation by protein phosphorylation. PLoS One *8*, e70692.

Cao, H., Bowling, S.A., Gordon, A.S., and Dong, X. (1994). Characterization of an *Arabidopsis* mutant that is nonresponsive to inducers of systemic acquired resistance. Plant Cell *6*, 1583–1592.

Ceci, M., Gaviraghi, C., Gorrini, C., Sala, L.A., Offenhäuser, N., Marchisio, P.C., and Biffo, S. (2003). Release of eIF6 (p27BBP) from the 60S subunit allows 80S ribosome assembly. Nature *426*, 579–584.

Chen, H., Zou, Y., Shang, Y., Lin, H., Wang, Y., Cai, R., Tang, X., and Zhou, J.-M. (2008). Firefly luciferase complementation imaging assay for protein-protein interactions in plants. Plant Physiol. *146*, 368–376.

Cheng, Z., Li, J.-F., Niu, Y., Zhang, X.-C., Woody, O.Z., Xiong, Y., Djonović, S., Millet, Y., Bush, J., McConkey, B.J., et al. (2015). Pathogen-secreted proteases activate a novel plant immune pathway. Nature *521*, 213–216.

Cho, H.Y., Lu, M.J., and Shih, M.C. (2019). The SnRK1-eIFiso4G1 signaling relay regulates the translation of specific mRNAs in *Arabidopsis* under submergence. New Phytol. *222*, 366–381.

Clark-Lewis, I., Sanghera, J.S., and Pelech, S.L. (1991). Definition of a consensus sequence for peptide substrate recognition by p44mpk, the meiosis-activated myelin basic protein kinase. J. Biol. Chem. *266*, 15180–15184.

Clough, S.J., and Bent, A.F. (1998). Floral dip: a simplified method for *Agrobacterium*-mediated transformation of *Arabidopsis thaliana*. Plant J. *16*, 735–743.

Duprat, A., Caranta, C., Revers, F., Menand, B., Browning, K.S., and Robaglia, C. (2002). The *Arabidopsis* eukaryotic initiation factor (iso)4E is dispensable for plant growth but required for susceptibility to potyviruses. Plant J. *32*, 927–934.

Echevarría-Zomeño, S., Yángüez, E., Fernández-Bautista, N., Castro-Sanz, A.B., Ferrando, A., and Castellano, M.M. (2013). Regulation of translation initiation under biotic and abiotic stresses. Int. J. Mol. Sci. *14*, 4670–4683.

Gilbert, W.V., Zhou, K., Butler, T.K., and Doudna, J.A. (2007). Cap-independent translation is required for starvation-induced differentiation in yeast. Science *317*, 1224–1227.

Hinnebusch, A.G., Ivanov, I.P., and Sonenberg, N. (2016). Translational control by 5′-untranslated regions of eukaryotic mRNAs. Science *352*, 1413–1416.

Holsters, M., Silva, B., Van Vliet, F., Genetello, C., De Block, M., Dhaese, P., Depicker, A., Inzé, D., Engler, G., and Villarroel, R. (1980). The functional organization of the nopaline *A. tumefaciens* plasmid pTiC58. Plasmid *3*, 212–230.

Izquierdo, Y., Kulasekaran, S., Benito, P., López, B., Marcos, R., Cascón, T., Hamberg, M., and Castresana, C. (2018). *Arabidopsis* nonresponding to oxylipins locus NOXY7 encodes a yeast GCN1 homolog that mediates noncanonical translation regulation and stress adaptation. Plant Cell Environ. *41*, 1438–1452.

Jackson, R.J., Hellen, C.U., and Pestova, T.V. (2010). The mechanism of eukaryotic translation initiation and principles of its regulation. Nat. Rev. Mol. Cell Biol. *11*, 113–127.

Kahvejian, A., Roy, G., and Sonenberg, N. (2001). The mRNA closed-loop model: the function of PABP and PABP-interacting proteins in mRNA translation. Cold Spring Harb. Symp. Quant. Biol. *66*, 293–300.

Karimi, M., De Meyer, B., and Hilson, P. (2005). Modular cloning in plant cells. Trends Plant Sci. *10*, 103–105.

Lellis, A.D., Allen, M.L., Aertker, A.W., Tran, J.K., Hillis, D.M., Harbin, C.R., Caldwell, C., Gallie, D.R., and Browning, K.S. (2010). Deletion of the eIFiso4G subunit of the *Arabidopsis* eIFiso4F translation initiation complex impairs health and viability. Plant Mol. Biol. *74*, 249–263.

Li, L., Li, M., Yu, L., Zhou, Z., Liang, X., Liu, Z., Cai, G., Gao, L., Zhang, X., Wang, Y., et al. (2014). The FLS2-associated kinase BIK1 directly phosphorylates the NADPH oxidase RbohD to control plant immunity. Cell Host Microbe *15*, 329–338.

Liang, X., Ma, M., Zhou, Z., Wang, J., Yang, X., Rao, S., Bi, G., Li, L., Zhang, X., Chai, J., et al. (2018). Ligand-triggered de-repression of *Arabidopsis* heterotrimeric G proteins coupled to immune receptor kinases. Cell Res. *28*, 529–543.

Liu, J., Elmore, J.M., Fuglsang, A.T., Palmgren, M.G., Staskawicz, B.J., and Coaker, G. (2009). RIN4 functions with plasma membrane H+-ATPases to regulate stomatal apertures during pathogen attack. PLoS Biol. *7*, e1000139.

Liu, X., Afrin, T., and Pajerowska-Mukhtar, K.M. (2019). *Arabidopsis* GCN2 kinase contributes to ABA homeostasis and stomatal immunity. Commun. Biol. *2*, 302.

Lokdarshi, A., Morgan, P.W., Franks, M., Emert, Z., Emanuel, C., and von Arnim, A.G. (2020). Light-dependent activation of the GCN2 kinase under cold and salt stress is mediated by the photosynthetic status of the chloroplast. Front. Plant Sci. *11*, 431.

Meng, X., and Zhang, S. (2013). MAPK cascades in plant disease resistance signaling. Annu. Rev. Phytopathol. *51*, 245–266.

Nicaise, V., Gallois, J.L., Chafiai, F., Allen, L.M., Schurdi-Levraud, V., Browning, K.S., Candresse, T., Caranta, C., Le Gall, O., and German-Retana, S. (2007). Coordinated and selective recruitment of eIF4E and eIF4G factors for Potyvirus infection in *Arabidopsis thaliana*. FEBS Lett. *581*, 1041–1046.

Niu, Y., and Sheen, J. (2012). Transient expression assays for quantifying signaling output. Methods Mol. Biol. *876*, 195–206.

Pajerowska-Mukhtar, K.M., Wang, W., Tada, Y., Oka, N., Tucker, C.L., Fonseca, J.P., and Dong, X. (2012). The HSF-like transcription factor TBF1 is a major molecular switch for plant growth-to-defense transition. Curr. Biol. *22*, 103–112.

Patrick, R.M., and Browning, K.S. (2012). The eIF4F and eIFiso4F complexes of plants: an evolutionary perspective. Comp. Funct. Genomics *2012*, 287814.

Patrick, R.M., Lee, J.C.H., Teetsel, J.R.J., Yang, S.-H., Choy, G.S., and Browning, K.S. (2018). Discovery and characterization of conserved binding of eIF4E 1 (CBE1), a eukaryotic translation initiation factor 4E–binding plant protein. J. Biol. Chem. *293*, 17240–17247.

Rasmussen, M.W., Roux, M., Petersen, M., and Mundy, J. (2012). MAP kinase cascades in *Arabidopsis* innate immunity. Front. Plant Sci. *3*, 169.

Schindelin, J., Arganda-Carreras, I., Frise, E., Kaynig, V., Longair, M., Pietzsch, T., Preibisch, S., Rueden, C., Saalfeld, S., Schmid, B., et al. (2012). Fiji: an open-source platform for biological-image analysis. Nat. Methods *9*, 676–682.

Schwab, R., Ossowski, S., Riester, M., Warthmann, N., and Weigel, D. (2006). Highly specific gene silencing by artificial microRNAs in *Arabidopsis*. Plant Cell *18*, 1121–1133.

SenGupta, J., Nilsson, J., Gursky, R., Spahn, C.M.T., Nissen, P., and Frank, J. (2004). Identification of the versatile scaffold protein RACK1 on the eukaryotic ribosome by cryo-EM. Nat. Struct. Mol. Biol. *11*, 957–962.

Sörensson, C., Lenman, M., Veide-Vilg, J., Schopper, S., Ljungdahl, T., Grøtli, M., Tamás, M.J., Peck, S.C., and Andreasson, E. (2012). Determination of primary sequence specificity of *Arabidopsis* MAPKs MPK3 and MPK6 leads to identification of new substrates. Biochem. J. *446*, 271–278.

Szklarczyk, D., Gable, A.L., Nastou, K.C., Lyon, D., Kirsch, R., Pyysalo, S., Doncheva, N.T., Legeay, M., Fang, T., Bork, P., et al. (2021). The STRING database in 2021: customizable protein–protein networks, and functional characterization of user-uploaded gene/measurement sets. Nucleic Acids Res. *49*, D605–D612.

Tarun, S.Z., Jr., and Sachs, A.B. (1995). A common function for mRNA 5′ and 3′ ends in translation initiation in yeast. Genes Dev. *9*, 2997–3007.

Tarun, S.Z., Jr., Wells, S.E., Deardorff, J.A., and Sachs, A.B. (1997). Translation initiation factor eIF4G mediates in vitro poly(A) tail-dependent translation. Proc. Natl. Acad. Sci. USA *94*, 9046–9051.

Wang, J., Grubb, L.E., Wang, J., Liang, X., Li, L., Gao, C., Ma, M., Feng, F., Li, M., Li, L., et al. (2018). A regulatory module controlling homeostasis of a plant immune kinase. Mol. Cell *69*, 493–504.e6.

Wells, S.E., Hillner, P.E., Vale, R.D., and Sachs, A.B. (1998). Circularization of mRNA by eukaryotic translation initiation factors. Mol. Cell *2*, 135–140.

Xu, G., Greene, G.H., Yoo, H., Liu, L., Marqués, J., Motley, J., and Dong, X. (2017). Global translational reprogramming is a fundamental layer of immune regulation in plants. Nature *545*, 487–490.

Xu, J., and Chua, N.H. (2012). Dehydration stress activates *Arabidopsis* MPK6 to signal DCP1 phosphorylation. EMBO J. *31*, 1975–1984.

Xu, J., Xie, J., Yan, C., Zou, X., Ren, D., and Zhang, S. (2014). A chemical genetic approach demonstrates that MPK3/MPK6 activation and NADPH oxidase-mediated oxidative burst are two independent signaling events in plant immunity. Plant J. *77*, 222–234.

Xu, J., Yang, J.Y., Niu, Q.W., and Chua, N.H. (2006). *Arabidopsis* DCP2, DCP1, and VARICOSE form a decapping complex required for postembryonic development. Plant Cell *18*, 3386–3398.

Xue, S., Tian, S., Fujii, K., Kladwang, W., Das, R., and Barna, M. (2015). RNA regulons in Hox 5′ UTRs confer ribosome specificity to gene regulation. Nature *517*, 33–38.

Yu, X., Li, B., Jang, G.J., Jiang, S., Jiang, D., Jang, J.C., Wu, S.H., Shan, L., and He, P. (2019). Orchestration of processing body dynamics and mRNA decay in *Arabidopsis* immunity. Cell Rep. *28*, 2194–2205.e6.

Zavaliev, R., Mohan, R., Chen, T., and Dong, X. (2020). Formation of NPR1 condensates promotes cell survival during the plant immune response. Cell *182*, 1093–1108.e18.

Zhang, J., Li, W., Xiang, T., Liu, Z., Laluk, K., Ding, X., Zou, Y., Gao, M., Zhang, X., Chen, S., et al. (2010). Receptor-like cytoplasmic kinases integrate signaling from multiple plant immune receptors and are targeted by a *Pseudomonas syringae* effector. Cell Host Microbe *7*, 290–301.

Zipfel, C., Kunze, G., Chinchilla, D., Caniard, A., Jones, J.D.G., Boller, T., and Felix, G. (2006). Perception of the bacterial PAMP EF-Tu by the receptor EFR restricts *Agrobacterium*-mediated transformation. Cell *125*, 749–760.

## STAR★METHODS

### KEY RESOURCES TABLE

| REAGENT or RESOURCE | SOURCE | IDENTIFIER |
|---|---|---|
| **Antibodies** | | |
| Mouse monoclonal anti-HA | BioLegend | Cat. #901502; RRID: AB_2565007 |
| Mouse monoclonal anti-HIS | Santa Cruz Biotechnology | Cat. #sc-8036, RRID: AB_627727 |
| Mouse monoclonal anti-FLAG | Sigma-Aldrich | Cat. #F1804, RRID: AB_262044 |
| Rabbit polyclonal anti-pSer566 | This paper | N/A |
| Rabbit polyclonal anti-pSer1066/1069 | This paper | N/A |
| Rabbit polyclonal anti-pSer487 | This paper | N/A |
| Rabbit polyclonal anti-pSer542 | This paper | N/A |
| **Bacterial and Fungal Strains** | | |
| *Agrobacterium tumefaciens GV3101* | Holsters et al. (1980) | N/A |
| *Escherichia coli* Top10 | Invitrogen | Cat#C4040 |
| *Pseudomonas syringae pv. maculicola (Psm) ES4326* | Cao et al. (1994) | N/A |
| *Escherichia coli* BL21 | NEB | Cat. #C2527H |
| **Chemicals, Peptides, and Recombinant Proteins** | | |
| 3× FLAG peptide | Sigma-Aldrich | Cat. #F4799 |
| Anti-Flag M2 Beads (affinity gel) | Sigma-Aldrich | Cat. #A2220, RRID: AB_10063035 |
| Estradiol | Sigma-Aldrich | Cat. #E8875 |
| D-Luciferin | BioVision | Cat. #7903 |
| Elf18 peptide | GenScript | Custom order |
| NA-PP1 | Sigma-Aldrich | Cat. #529579 |
| Terminator™ 5′-Phosphate-Dependent Exonuclease | Lucigen | Cat. #TER51020 |
| Phos-tag (TM) Acrylamide | FUJIFILM Wako | Cat. #304-93521 |
| Amino Acid Mixture, Complete | Promega | Cat. #L4461 |
| m7G(5')ppp(5')G RNA Cap Structure Analog | NEB | Cat. #S1404S |
| SUPERase•In RNase Inhibitor | Invitrogen | Cat. #AM2694 |
| RiboLock RNase Inhibitor | Thermo Scientific | Cat. #EO0382 |
| Proteinase K | Thermo Scientific | Cat. #EO0491 |
| RNase H | Thermo Scientific | Cat. #EN0201 |
| Ppase | NEB | Cat. #P0753L |
| Protease Inhibigtor Cocktail Tablets | Roche | Cat. #04693116001 |
| **Critical Commercial Assays** | | |
| Dual Luciferase Reporter Assay System | Promega | Cat. #E1910 |
| Wheat Germ Extract | Promega | Cat. #L4380 |
| RiboMAX Large Scale RNA Production Systems | Promega | Cat. #P1300 |
| Vaccinia Capping System | NEB | Cat. #M2080S |
| **Experimental Models: Organisms/Strains** | | |
| *Arabidopsis: 35S:DCP2-HA (DCP2OE-HA)* | *This paper* | *N/A* |
| *Arabidopsis: dcp2-1 35S:DCP2-HA* | *This paper* | *N/A* |
| *Arabidopsis: dcp2-1 35S:DCP2 (E158Q)-HA* | *This paper* | *N/A* |
| *Arabidopsis: dcp2-1* | NASC | *N/A* |
| *Arabidopsis: vcs-7* | NASC | N/A |
| *Arabidopsis: estradiol:amiR-DCP2* | This paper | N/A |
| *Arabidopsis: pab2.5 (pab2 pab8 plus heterozygous pab4)* | This paper | N/A |
| *Arabidopsis: pab2 pab4* | Xu et al. (2017) | N/A |

(*Continued on next page*)

*Continued*

| REAGENT or RESOURCE | SOURCE | IDENTIFIER |
|---|---|---|
| *Arabidopsis: pab2 pab8* | Xu et al. (2017) | N/A |
| *Arabidopsis: eif4g eif4e1* | This paper | N/A |
| *Arabidopsis: eif4g* | Nicaise et al. (2007) | N/A |
| *Arabidopsis: eif4e1* | Patrick et al. (2018) | N/A |
| *Arabidopsis: eifiso4g1 eifiso4g2* | Nicaise et al. (2007) | N/A |
| *Arabidopsis: eifiso4e* | Duprat et al. (2002) | N/A |
| *Arabidopsis: pab2 pab8 eif4g eif4e1* | This paper | N/A |
| *Arabidopsis: pab2 pab4 eifiso4g1 eifiso4g2* | This paper | N/A |
| *Arabidopsis: rack1-es 1 and 2* | Cheng et al. (2015) | N/A |
| *Arabidopsis*: pab2 pab8 rack1-es2 | This paper | N/A |
| *Arabidopsis*: eif4g eif4e1 rack1-es2 | This paper | N/A |
| *Arabidopsis: eifiso4g1 eifiso4g2 rack1-es2* | This paper | N/A |
| *Arabidopsis: mpk6SR* | Xu et al. (2014) | N/A |
| *Arabidopsis: efr-1* | Zipfel et al. (2006) | N/A |
| *Arabidopsis: pab2 pab8 mpk6SR* | This paper | N/A |
| *Arabidopsis: pab2 pab8 NP:PAB8-HA* | This paper | N/A |
| *Arabidopsis: pab2 pab8 NP:PAB8$^{S566A}$-HA* | This paper | N/A |
| *Arabidopsis: pab2 pab8 NP:PAB8$^{S566D}$-HA* | This paper | N/A |
| *Arabidopsis: pab2 pab4 NP:PAB2-HA* | This paper | N/A |
| *Arabidopsis: pab2 pab4 NP:PAB4-HA* | This paper | N/A |
| *Arabidopsis: eif4g eif4e1 mpk6SR* | This paper | N/A |
| *Arabidopsis: eifiso4g1 eifiso4g2 NP:I4G1-HA* | This paper | N/A |
| *Arabidopsis: eifiso4g1 eifiso4g2 NP:I4G1$^{2A}$-HA* | This paper | N/A |
| *Arabidopsis: eifiso4g1 eifiso4g2 NP:I4G1$^{2D}$-HA* | This paper | N/A |
| *Arabidopsis*: 35S:uORF/R$_{TBF1}$-FLUC (WT) | This paper | N/A |
| *Arabidopsis*: 35S:uORF/mR123$_{TBF1}$-FLUC (mR123) | This paper | N/A |
| *Arabidopsis*: 35S:uORF/mR3$_{TBF1}$-FLUC (mR3) | This paper | N/A |
| Oligonucleotides | | |
| Primers see Table S4 | Invitrogen | Custom order |
| Recombinant DNA | | |
| pET28a | EMD Biosciences | 69864-3 |
| pGEX 6P-1 | Amersham Biosciences | 27-4597-01 |
| pET28a-MPK6-HIS | Bi et al. (2018) | N/A |
| pGEX 6P-1-GST-PAB8 | This paper | N/A |
| pGEX 6P-1-GST-PAB8$^{S566A}$ | This paper | N/A |
| pGEX 6P-1-GST-eIF4G | This paper | N/A |
| pGEX 6P-1-GST-eIF4G$^{8A}$ | This paper | N/A |
| pGEX 6P-1-GST-eIFiso4G1 | This paper | N/A |
| pGEX 6P-1-GST-eIFiso4G1$^{2A}$ | This paper | N/A |
| pCAMBIA1300 | Wang et al. (2018) | N/A |
| pCAMBIA-35S-DCP2-HA | This paper | N/A |
| pCAMBIA-35S-DCP2$^{E158Q}$-HA | This paper | N/A |
| pCAMBIA-pPAB2:PAB2-HA | This paper | N/A |
| pCAMBIA-pPAB4:PAB4-HA | This paper | N/A |
| pCAMBIA-35S-PAB8-HA | This paper | N/A |
| pCAMBIA-35S-PAB8$^{S566A}$-HA | This paper | N/A |
| pCAMBIA-35S-PAB8$^{S566D}$-HA | This paper | N/A |
| pCAMBIA-pPAB8:PAB8-HA | This paper | N/A |
| pCAMBIA-pPAB8:PAB8$^{S566A}$-HA | This paper | N/A |

(*Continued on next page*)

*Continued*

| REAGENT or RESOURCE | SOURCE | IDENTIFIER |
|---|---|---|
| pCAMBIA-pPAB8:PAB8$^{S566D}$-HA | This paper | N/A |
| pCAMBIA-35S-PAB8-HA-MS2 | This paper | N/A |
| pCAMBIA-35S-eGFP-HA-MS2 | This paper | N/A |
| pCAMBIA-35S-eIF4G-HA | This paper | N/A |
| pCAMBIA-35S-eIF4G$^{8A}$-HA | This paper | N/A |
| pCAMBIA-35S-eIF4G$^{8D}$-HA | This paper | N/A |
| pCAMBIA-35S-eIFiso4G1-HA | This paper | N/A |
| pCAMBIA-35S- eIFiso4G1$^{2A}$-HA | This paper | N/A |
| pCAMBIA-35S- eIFiso4G1$^{2D}$-HA | This paper | N/A |
| pCAMBIA-peIFiso4G1:eIFiso4G1-HA | This paper | N/A |
| pCAMBIA-peIFiso4G1:eIFiso4G1$^{2A}$-HA | This paper | N/A |
| pCAMBIA-peIFiso4G1:eIFiso4G1$^{2D}$-HA | This paper | N/A |
| pCAMBIA-35S- Cluc-PAB2 | This paper | N/A |
| pCAMBIA-35S- Cluc-PAB4 | This paper | N/A |
| pCAMBIA-35S- Cluc-PAB8 | This paper | N/A |
| pCAMBIA-35S- Cluc-CPR5 | Wang et al. (2018) | N/A |
| pCAMBIA-35S-Cluc-RACK1A | This paper | N/A |
| pCAMBIA-35S-Cluc-RACK1B | This paper | N/A |
| pCAMBIA-35S-Cluc-RACK1C | This paper | N/A |
| pCAMBIA-35S-Cluc-MPK3 | This paper | N/A |
| pCAMBIA-35S-Cluc-MPK6 | This paper | N/A |
| pCAMBIA-35S-BAK1-Nluc | Wang et al. (2018) | N/A |
| pCAMBIA-35S-eIF4G-Nluc | This paper | N/A |
| pCAMBIA-35S-eIFiso4G1-Nluc | This paper | N/A |
| pCAMBIA-35S-PAB8-Nluc | This paper | N/A |
| pBm43GW | Karimi et al. (2005) | N/A |
| pBm43GW-amiR-DCP2 | This paper | N/A |
| WT TBF1: 35S:uORF/$R_{TBF1}$-FLUC/35S:RLUC | This paper | N/A |
| mR123: 35S:uORF/mR123$_{TBF1}$-FLUC/35S:RLUC | This paper | N/A |
| mR1: 35S:uORF/mR1$_{TBF1}$-FLUC/35S:RLUC | This paper | N/A |
| mR2: 35S:uORF/mR2$_{TBF1}$-FLUC/35S:RLUC | This paper | N/A |
| mR3: 35S:uORF/mR3$_{TBF1}$-FLUC/35S:RLUC | This paper | N/A |
| ZIK3: pGX731 | Xu et al. (2017) | N/A |
| ATG8E: pGX728 | Xu et al. (2017) | N/A |
| uorf: 35S:uorf/$R_{TBF1}$-FLUC/35S:RLUC | This paper | N/A |
| uorf/mR123: 35S:uorf/mR123$_{TBF1}$-FLUC/35S:RLUC | This paper | N/A |
| TIE-uorf: 35S:TIE-uorf/$R_{TBF1}$-FLUC/35S:RLUC | This paper | N/A |
| TIE-uorf/mR123: 35S:TIE-uorf/mR123$_{TBF1}$-FLUC/35S:RLUC | This paper | N/A |
| Bicistronic-uorf: 35S:RLUC-uorf/$R_{TBF1}$-FLUC | This paper | N/A |
| Bicistronic-uorf/mR123: 35S:RLUC-uorf/m$R_{TBF1}$-FLUC | This paper | N/A |
| M6-uorf/mR123: 35S:M6-uorf/mR123$_{TBF1}$-FLUC/35S:RLUC | This paper | N/A |
| pGX664: 35S:EFR–EGFP | Xu et al. (2017) | N/A |
| pUC19-35S-PAB2-FLAG | This paper | N/A |
| pUC19-35S-PAB2-HA | This paper | N/A |
| pUC19-35S-PAB8-FLAG | This paper | N/A |
| pUC19-35S-PAB8-HA | This paper | N/A |
| pUC19-35S-PAB8$^{S566A}$-HA | This paper | N/A |
| pUC19-35S-PAB8$^{S566A}$-FLAG | This paper | N/A |
| pUC19-35S-PAB8$^{S566D}$-FLAG | This paper | N/A |

(*Continued on next page*)

| Continued | | |
|---|---|---|
| REAGENT or RESOURCE | SOURCE | IDENTIFIER |
| pUC19-35S-eIFiso4G1-FLAG | This paper | N/A |
| pUC19-35S-eIFiso4G1-HA (WT and mutant variants) | This paper | N/A |
| pUC19-35S-eIF4G-FLAG | This paper | N/A |
| pUC19-35S-eIF4G-HA (WT, mutant and truncation variants) | This paper | N/A |
| pUC19-35S-RACK1A-HA | This paper | N/A |
| pUC19-35S-MPK6-HA | This paper | N/A |
| Software and Algorithms | | |
| ImageJ | Schindelin et al. (2012) | https://imagej.nih.gov/ij/ |
| Prism 8 | GraphPad | https://www.graphpad.com/ |

## RESOURCE AVAILABILITY

### Lead contact

Further information and requests for reagents may be directed to and will be fulfilled by the lead contact Xinnian Dong (xdong@duke.edu).

### Materials availability

All unique constructs and reagents in this study are available from the lead contact upon completion of Materials Transfer Agreement.

### Data and code availability

- All data reported in this paper will be shared by the lead contact upon request.
- This study generated a dataset provided in Table S3 and did not report original code.
- Any additional information required to reanalyze the data reported in this work paper is available from the lead contact upon request.

## EXPERIMENTAL MODEL AND SUBJECT DETAILS

*Arabidopsis* plants used in this study are all in the Col-0 (WT) background. *Arabidopsis* plants were grown in soil at 22 °C in a 12/12 h light/dark photoperiod with 60% relative humidity for 3-4 weeks before experiments. Wild-type (WT) *Nicotiana benthamiana* (*Nb*) plants were grown under the same conditions for 5-6 weeks before being used for transient assays. Previously published lines are: *pab2 pab4* (Xu et al., 2017), *pab2 pab8* (Xu et al., 2017), *eif4g* (Nicaise et al., 2007), *eif4e1* (Patrick et al., 2018), *eifiso4g1 eifiso4g2* (Nicaise et al., 2007), *eifiso4e* (Duprat et al., 2002), *rack1-es1/2* (Cheng et al., 2015), *mpk6SR* (Xu et al., 2014) and *efr-1* (Zipfel et al., 2006). T-DNA insertion mutants *dcp2-1* (*SALK_000519*) and *vcs-7* (*N66965*) were obtained from the European *Arabidopsis* Stock Centre (NASC). *DCP2OE-HA* and *amiR-DCP2 Arabidopsis* transgenic lines were generated in the WT background; the *35S:DCP2-HA* and *35S:DCP2$^{E158Q}$-HA* lines in the *dcp2-1* mutant background; the *NP:PAB8-HA*, *NP:PAB8$^{S566A}$-HA* and *NP:PAB8$^{S566D}$-HA* lines in *pab2 pab8*; *NP:PAB2-HA* and *NP:PAB4-HA* lines in *pab2 pab4*; the *NP:I4G1-HA*, *NP:I4G1$^{2A}$-HA* and *NP:I4G1$^{2D}$-HA* lines in *eifiso4g1 eifiso4g2*; and the *35S:uORF/R$_{TBF1}$-FLUC* (*WT*), *35S:uORF/mR123$_{TBF1}$-FLUC* (*mR123*) and *35S:uORF/mR3$_{TBF1}$-FLUC* (*mR3*) lines in the WT background. All transgenic lines used in this study are in the T3 generation. High-order mutants (*pab2.5*, *eif4g eif4e1*, *pab2 pab8 eif4g eif4e1*, *pab2 pab4 eifiso4g1 eifiso4g2*, *pab2 pab8 rack1-es2*, *eif4g eif4e1 rack1-es2*, *eifiso4g1 eifiso4g2 rack1-es2*, *pab2 pab8 mpk6SR* and *eif4g eif4e1 mpk6SR*) were generated by genetic crossing.

## METHOD DETAILS

### Plasmid construction

To generate *35S:DCP2-HA*, *35S:DCP2$^{E158Q}$-HA* and *35S:DCP2OE-HA* transgenic plants in the *dcp2-1* mutant background, the DCP2 fragment were PCR-amplified from WT cDNA and cloned into the pCAMBIA1300-35S:HA-RBS plasmid. The *estradiol*-inducible *DCP2* knockdown transgenic plants, *amiR-DCP2*, were generated using 21mer artificial microRNA (*amiR*) designed following a previous report (Schwab et al., 2006) and used to replace the corresponding region of the *Arabidopsis*-derived miR319a by overlapping PCR, and the resulting recombinant miR319a containing the designed artificial microRNA targeting *DCP2* (amiR-DCP2) was cloned into pBm43GW vector following a previous report (Karimi et al., 2005). To generate FLAG- or HA-tagged PAB2, PAB8, eIF4G, eIFiso4G1, RACK1A, and MPK6 constructs for transient expression in protoplasts, the corresponding coding sequences

(CDSs) were PCR-amplified from WT cDNA and introduced into the PUC19-35S:FLAG/HA-RBS vector by either ligation or In-fusion cloning (Takara). Point mutations of PAB8, eIF4G and eIFiso4G1 were generated using the QuikChange II site-directed mutagenesis kit (Agilent). The *TBF1* leader sequence was PCR-amplified from the genomic DNA, the R-motif point mutant variants in the leader sequence (*mR1*, *mR2*, *mR3* and *mR123*) were synthesized by IDT (Table S2), the TIE sequence (170 nt) was PCR-amplified from the RLUC-Hoxa3 5′ UTR FLUC construct (Xue et al., 2015) and fused with the *TBF1* 5′ leader sequence with either the uORF mutant (*uorf*) or the uORF and R-motif mutant (*uorf/mR123*) by overlapping PCR. The resulting fragments were cloned into the pGX plasmid (Xu et al., 2017) by ligation. For the bicistronic assay, the *RLUC* and *FLUC* sequences were PCR-amplified and fused by overlapping PCR. The resulting fragments were cloned into the pGX plasmid (Xu et al., 2017) by ligation to generate a bicistronic construct. The *TBF1* 5′ leader sequence with either the *uORF* mutations (*uorf*) or the *uORF* and R-motif mutations (*uorf/mR123*) was inserted into the bicistronic construct between *RLUC* and *FLUC* sequences by ligation cloning. For the MS2 tethering assay, *MS2* and 6x MS2 binding sites (*M6*) sequences were PCR-amplified from plasmids pMS2-YFP and pSL-MS2-6x (Bertrand et al., 1998), respectively. The resulting *MS2* fragment was ligated into pCAMBIA-35S-PAB8-HA and the *M6* fragment was introduced into the *uorf/mR123* dual reporter by In-fusion cloning. To generate a control for PAB8-HA-MS2 protein, *eGFP* was PCR-amplified and ligated into the pCAMBIA-35S-PAB8-HA-MS plasmid to replace the *PAB8* fragment. For the split-luciferase assay, CDSs with the FLAG tag were PCR-amplified from the corresponding PUC19 constructs and introduced into pCAMBIA-Cluc or pCAMBIA-Nluc (Chen et al., 2008) by either ligation or In-fusion cloning. Cluc-CPR5 and BAK1-Nluc were previously described (Liang et al., 2018; Wang et al., 2018). For the dual luciferase assay, CDSs of PAB8, eIF4G, eIFiso4G1 and their phosphorylation variants were PCR-amplified from the corresponding PUC19 vectors and cloned into the pCAMBIA1300-35S:HA-RBS plasmid through ligation or In-fusion cloning. *ZIK3* (pGX731) and *ATG8E* (pGX728) were previously reported (Xu et al., 2017). To generate *NP:PAB2-HA* and *NP:PAB4-HA* transgenic plants in *pab2 pab4*, a fragment containing about 1 kb native promoter (*NP*) of *PAB2* or *PAB4* with their corresponding CDS was PCR-amplified from WT genomic DNA and cloned into the pCAMBIA1300-HA-RBS vector by In-fusion cloning. For generating *PAB8* and *eIFiso4G1* transgenic plants containing mutated phosphosites, a fragment containing about 1.3 kb native promoter of *PAB8* or *eIFiso4g1* fused with their corresponding CDS was cloned into the pCAMBIA1300-HA-RBS vector. Point mutations of *DCP2*, *PAB8* and *eIFiso4G1* were generated using the QuikChange II site-directed mutagenesis kit (Agilent) and introduced into WT, *dcp2-1*, *pab2 pab4*, *pab2 pab8* or *eifiso4g1 eifiso4g2* mutant plants correspondingly by *Agrobacterium*-mediated transformation (Clough and Bent, 1998). The GST fusion constructs were generated using CDSs of desired genes amplified by PCR and cloned into the pGEX 6P-1 vector (Wang et al., 2018). MPK6-HIS was previously reported (Bi et al., 2018). The primers used and the restriction enzyme information needed for plasmid construction are listed in Table S4.

### Confocal laser scanning microscopy

*Agrobacterium* strain GV3101 carrying indicated construct was cultured for 12 h at 28 °C, 220 rpm in 2 mL Luria-Bertani (LB) broth with 50 μg/mL kanamycin, gentamycin and rifampicin before secondary propagation in 15 mL LB broth supplied with same antibiotics and 200 μM acetosyringone. After overnight incubation, bacteria were spun down at 2,000 g for 5 min, washed once, and resuspended in the infiltration buffer [10 mM 2-(N-morpholino) ethanesulfonic acid (MES), 10 mM $MgCl_2$, 200 μM acetosyringone] at $OD_{600nm}$ = 0.6 before infiltration into fully expanded *Nb* leaves. The imaging was performed with the Zeiss 880 Airyscan inverted confocal laser scanning microscope using a 40x/1.2 water correction objective. YFP was excited through a 488 nm argon laser, and emission was recorded with a 516-544 nm band pass filter. mCherry was excited through a 561 nm DPSS laser, and emission was detected with a 592-629 nm band pass filter. A spectral GaAsP detector was used to collect emission from YFP when YFP and mCherry were imaged together.

### Decapping assay, RNA isolation and qPCR

8-day-old seedlings (20/sample) grown on solid ½ MS were transferred to 1 mL liquid ½ MS overnight before adding another 1 mL liquid ½ MS with mock or 20 μM elf18 for 1 h. Total mRNA (Control) was extracted from the mock- and elf18- treated seedlings using TRIzol (Invitrogen). For exonuclease-based decapping assay, 10 μg of each sample was exposed to 1 U exonuclease (Lucigen) at 42 °C for 30 min. The exonuclease-treated mRNA was purified using RNeasy MinElute Cleanup Kit (Qiagen) and subjected to reverse transcription together with the control mRNA using the First-strand cDNA Synthesis Kit (Thermo) following the manufacturer's manual before qPCR was performed using FastStart Universal SYBR Green Master Kit (Roche). Decapping was measured by the ratio of exonuclease-treated mRNA normalized to the untreated control mRNA. For cap recognition antibody-based decapping assay, 200 μL protein A agarose (Millipore) was washed 3 times with 1 mL of ice-cold IPP buffer (150 mM NaCl, 0.1% Triton X-100, 50 mM Tris-HCl, pH 7.4). Half of the agarose was resuspended in 250 μL IPP buffer with 0.2 U/μL SUPERase•In RNase Inhibitor (Invitrogen) and treated overnight at 4 °C with rotations (non-coated beads). The other half of the agarose was resuspended in 250 μL IPP buffer with 8 μL anti-m7G-cap mouse monoclonal antibody (Synaptic Systems) and incubated for 3 h at 4 °C with rotations. The antibody-conjugated protein A beads were further incubated with 50 U RNase inhibitor (Invitrogen) at 4 °C overnight with rotations (antibody-coated beads) and washed 5 times with 1 mL ice-cold IPP buffer before resuspension in 100 μL IPP buffer. 2 μg of RNA was added to the non-coated beads for 1 h at 4 °C to remove the background bindings. The RNA/beads slurry was then centrifuged at 700 g, 4 °C for 2 min. The resulting supernatant was added to the 100 μL antibody-coated beads and incubated at 4 °C overnight with rotations with 0.5 M random decamers (Invitrogen, Japan) as blocking reagent. The resulting beads (capped RNA) were washed 5 times with 1 mL ice-cold IPP buffer and centrifuged at 700 g, 4 °C for 2 min. The capped RNA was extracted

from the final pellet using 1 mL TRIzol and subjected to RT-PCR with the total RNA without cap antibody purification as input. The primers used are listed in Table S4.

### Elf18-induced growth inhibition assay

Elf18-induced growth inhibition assay was performed as previously described (Xu et al., 2017) with modifications. Seeds were sterilized in a 20% Germicidal Bleach solution (CLOROX) for 10 min and washed 5 times with sterilized water before sowing on solid ½ Murashige & Skoog (MS). 5-day-old seedlings (6-10/sample) were transferred to liquid ½ MS overnight in the presence of 50 μM estradiol (for estradiol-inducible transgenes) or 2 μM NA-PP1 (for the inhibitor-sensitized MPK3 variant-rescued *mpk3 mpk6* double mutant, *mpk6SR*), then treated with mock or 100 nM elf18, and fresh weight was measured 3-4 days after the treatment.

### Luciferase reporter assay

Luciferase assay in *Arabidopsis* plants was performed through CCD imaging as previously described (Xu et al., 2017) with modifications. In brief, 3-4-week-old independent *Arabidopsis* transgenic lines carrying the dual luciferase *35S:uORF/R$_{TBF1}$-FLUC/35S:RLUC* (WT), *35S:uORF/mR123$_{TBF1}$-FLUC/35S:RLUC* (*mR123*) or the *35S:uORF/mR3$_{TBF1}$-FLUC/35S:RLUC* (*mR3*) reporter were sprayed with 2 mM luciferin overnight before infiltration with either 10 μM elf18 or water for 1 h. Luciferase activity was measured using a CCD camera with 20 min exposure time. Dual luciferase assay in *Nb* plants was performed as previously described (Xu et al., 2017) with modifications. Briefly, after 3 h incubation at room temperature in the infiltration buffer [10 mM 2-(N-morpholino) ethanesulfonic acid (MES), 10 mM $MgCl_2$, 200 μM acetosyringone], *Agrobacterium tumefaciens* strain GV3101 containing the indicated construct was infiltrated into fully expanded *Nb* leaves at $OD_{600nm}$ = 0.1, except for the EFR-GFP strain ($OD_{600nm}$ = 0.2). For elf18 induction, the dual luciferase reporter strain ($OD_{600nm}$ = 0.1) and the elf18 receptor EFR-GFP strain ($OD_{600nm}$ = 0.2) were coinjected into *Nb* leaves, after 20 h, one half of the leaf was infiltrated with water (mock) while the other half was infiltrated with 10 μM elf18. After 2 h, leaf discs were collected, ground in liquid nitrogen and lysed with the PLB buffer (Promega, E1910). For the bicistronic assay, *Agrobacterium* strains containing the bicistronic reporter ($OD_{600nm}$ = 0.4) and EFR-GFP construct ($OD_{600nm}$ = 0.2) were co-infiltrated into *Nb* leaves. After 20 h, water or 10 μM elf18 was infiltrated into either half of a *Nb* leaf and leaf discs were collected after 2 h, ground in liquid nitrogen and dual luciferase assay was performed (Promega, E1910). For testing the effect of PABPs, eIF4G and eIFiso4G on the *TBF1* dual luciferase reporter translation in *Nb* plants, *Agrobacterium* containing the reporter was mixed with those carrying the indicated (Test) constructs or HA-mCherry (CK) at a ratio of 1:1. After 3 h of incubation, half of the *Nb* leaf was infiltrated with TBF1/CK, and the other half was infiltrated with TBF1/Test. After 2 days, leaf discs were collected, lysed with the PLB buffer and used for dual luciferase assay. To test if PAB8 promotes translation through the MS2 tethering system, *Agrobacterium* ($OD_{600nm}$ = 0.2) containing the *M6-uorf/mR123* reporter was mixed with those carrying *PAB8-HA-MS2*, *eGFP-HA-MS2*, *PAB8-HA* or *HA-mCherry* construct at a ratio of 1:1. After 3 h, half of the *Nb* leaf was infiltrated with either *M6-uorf/mR123/eGFP-HA-MS2* or *M6-uorf/mR123/HA-mCherry*, and the other half was infiltrated with *M6-uorf/mR123/PAB8-HA-MS2* or *M6-uorf/mR123/PAB8-HA* correspondingly. After 2 days, leaf discs were collected, lysed with the PLB buffer and dual luciferase assay was performed. For translation assay in protoplasts, 20-40 μg of the indicated the dual luciferase reporter was delivered into 300 μL protoplasts by PEG-mediated transfection (Niu and Sheen, 2012) and incubated overnight in the WI buffer (0.5 M mannitol, 4 mM MES, 20 mM KCl, pH 5.7) for assays without induction or W5 buffer (154 mM NaCl, 125 mM $CaCl_2$, 5 mM KCl, 2 mM MES, pH 5.7) for assays with elf18 induction. For non-induction assay, samples were collected at 2,000 g for 30 sec after overnight incubation. For elf18 induction assay, protoplasts were treated with 1 μM elf18 for 45 min before collection at 2,000 g for 30 sec. The collected protoplasts were lysed with the PLB buffer and 10 μL of the supernatant was taken for luciferase signal capture in a Victor3 plate reader (PerkinElmer) using previously reported settings (Xu et al., 2017).

### *In vitro* translation assay in wheat-germ system

The template DNA used for *in vitro* transcription was amplified by overlapping PCR using the primers listed in Table S4, and 2 μg of purified template DNA was subjected to *in vitro* transcription for 4 h using the RiboMAX™ Large Scale RNA Production Systems (Promega) following the manufacturer's instruction. The transcribed mRNA was capped using the Vaccinia Capping System (New England Biolabs). mRNA was purified using RNeasy MinElute Cleanup Kit (Qiagen) and translated in the wheat-germ system (Promega) following the manufacturer's instruction. Briefly, 1 μg of mRNA was incubated at 67 °C for 10 min and immediately cooled down on ice for 5 min before being added into a 20 μL reaction system, including 10 μL wheat-germ extract, 0.08 mM amino acid mixture, 60 mM potassium acetate and 0.8 U/μL RNase inhibitor (Invitrogen). The translation reaction was incubated at 25 °C for 60-90 min followed by addition of 100 μL 1 mM luciferin (BioVision) for luciferase measurement using the Victor3 plate reader (PerkinElmer).

### PABP/R-motif binding assay

*Arabidopsis* protoplasts were used for the purification of the FLAG-tagged PAB8 and phospho-sites variants as previously described (Niu and Sheen, 2012) with modifications. In brief, 3 mL protoplasts (from 5-10 fully-expanded leaves digested in 3 mL enzyme solution) were transfected with 200 μg indicated plasmids, incubated overnight and treated with or without 1 μM elf18 for indicated time. Samples were collected at 2,000 g for 30 sec and lysed with 1 mL of the extraction buffer [50 mM HEPES (pH 7.5), 150 mM KCl, 1 mM EDTA, 0.3% Triton-X 100, 1 mM DTT, 1× proteinase inhibitor cocktail (Roche)]. After centrifuging at 16,000 g for 15 min, the supernatant was incubated with 50 μL agarose-conjugated anti-FLAG antibody (Sigma) for 4 h at 4 °C with rotations. The precipitates were

washed 6 times with the washing buffer [50 mM HEPES (pH 7.5), 150 mM KCl, 1 mM EDTA, 0.2% Triton-X 100] before elution with 60 μL of 20 μg/mL 3× FLAG peptide (Sigma) for 1 h. The purified protein concentration was determined using Qubit™ Protein Assay Kit (Invitrogen). 5′ biotin-conjugated RNA probes were synthesized by IDT and listed in Table S2. For the PABP/R-motif binding assay, 10 μL Dynabeads™ M-280 Streptavidin (Invitrogen) was pre-treated in 1 mL of the washing buffer [50 mM HEPES (pH 7.5), 150 mM KCl, 1 mM EDTA, 0.2% Triton-X 100] supplied with 2% BSA at 4 °C for 2 h with rotations, then 0.2-0.4 nmol biotin-conjugated RNA probes were added to the bead slurry and incubated for another 2 h in the presence of 200 U/mL RNase inhibitors (Invitrogen). The RNA probe-coated beads were washed 3 times with 1 mL ice-cold extraction buffer [50 mM HEPES (pH 7.5), 150 mM KCl, 1 mM EDTA, 0.3% Triton-X 100, 1 mM DTT, 1× proteinase inhibitor cocktail (Roche)], followed by resuspension in 600 μL extraction buffer, addition of 200 U/mL RNase inhibitor and 9 μg plant-purified FLAG-tagged protein and incubation overnight at 4 °C with rotations. The resulting beads were washed 5 times using 1 mL ice-cold washing buffer and resuspended in 20 μL 1× protein loading buffer before 10 min 95 °C treatment for subsequent immunoblotting.

### LC-MS/MS analysis

The LC-MS/MS analysis was performed as previously reported (Liu et al., 2009) with modifications. Briefly, to identify PABP-associated proteins, 96 mL protoplasts transfected with 4.8 mg of pUC19-35S:PAB2-FLAG or pUC19-35S:FLAG-RBS (negative control) overnight were lysed with 15 mL buffer I [50 mM HEPES (pH 7.5), 50 mM NaCl, 10 mM EDTA, 0.2% Triton X-100, 0.1 mg/mL Dextran (Sigma), 1× proteinase inhibitor cocktail (Roche)]. The lysate was centrifuged at 13,000 rpm for 15 min, and the supernatant was filtered through a 0.22 μm filter (Millipore) followed by addition of 60 μL anti-FLAG agarose beads (Sigma) and incubation at 4 °C for 4 h with rotations. After immunoprecipitation, the beads were washed 2 times with buffer II (50 mM HEPES pH7.5, 50 mM NaCl, 10 mM EDTA, 0.1% Triton X-100), and 2 times with buffer III (50 mM HEPES pH7.5, 150 mM NaCl, 10 mM EDTA, 0.1% Triton X-100). The immunoprecipitates were then eluted with 75 μL of 20 μg/mL 3× FLAG peptide (Sigma) for 1 h and submitted to the Duke Proteomics Core Facility for trypsin digestion and LC-MS/MS analysis as previously described (Li et al., 2014; Zavaliev et al., 2020). To identify the elf18-induced phosphosites in PAB8, eIF4G and eIFiso4G1, protoplasts expressing FLAG-tagged PAB8, eIF4G or eIFiso4G1 were treated with 1 μM elf18 for 10 min before protein extraction. The eluted proteins were separated in 4-12% (FLAG-tagged PAB8 and eIFiso4G1) and 3-8% (eIF4G-FLAG) NuPAGE gel (Invitrogen), digested with trypsin, and subject to mass spectrometric analysis after phosphopeptide enrichment using TiO2.

### STRING analysis

Proteins in Table S3 were submitted to the STRING tool (Szklarczyk et al., 2021) to search for potential "hub proteins" linking PABPs and the translation initiation complex using text-mining, coexpression and experimental determination as active interaction sources. The interaction score was set to 0.700.

### Split-luciferase assay and co-IP assay

The split-luciferase assay was performed as previously described (Chen et al., 2008). In brief, *Agrobacterium tumefaciens* strain GV3101 containing indicated construct was infiltrated into fully expanded *Nb* leaves at $OD_{600nm}$ = 0.1. Leaf discs were taken after 2 days and incubated with 1 mM luciferin in a 96-well plate for 15 min. Luminescence was captured for 1 sec using the Victor3 plate reader (PerkinElmer). To detect the dynamic interaction of PABPs with eIF4G or eIFiso4G1, leaf discs were treated with 10 μM elf18 or water in the presence of 1 mM luciferin before luciferase measurement at the indicated times.

The co-IP assay was performed as in the PABP/R-motif binding assay. Briefly, 100-200 μg of indicated constructs were delivered into 3 mL protoplasts (from 5-10 fully expanded leaves digested in 3 mL enzyme solution) by PEG-mediated transfection (Niu and Sheen, 2012), incubated overnight and treated with water or 1 μM elf18 for 10 min. Samples were collected and lysed with 1 mL of the extraction buffer. After centrifuging at 16,000 g for 15 min, 60 μL supernatant was taken as input, and the rest of the sample was used to affinity-purify the co-IP complex through agarose-conjugated anti-FLAG antibody and eluted with 3× FLAG peptide before immunoblotting.

### Elf18-induced infection protection assay

Elf18-induced protection assay was performed as previously described (Zhang et al., 2010) with modifications, 3- to 4-week-old plants were pre-treated with water (mock) or 1 μM elf18 for 1 day, or pre-treated with 50 μM estradiol (for estradiol-inducible transgenes) for 1 day before treatment with mock or 1 μM elf18 in the presence of 50 μM estradiol for another day followed by inoculation with *Psm* ES4326 at $OD_{600nm}$ = 0.001. After another 2 days, bacterial titer in the leaf was determined by serial dilutions in 10 mM $MgCl_2$ solution.

### Phos-tag gel assay

For phos-tag gel assay of protoplast-produced proteins, 15-20 μg of indicated constructs were introduced into 300 μL protoplasts prepared from WT or mutant plants, incubated overnight with or without 50 μM estradiol (*rack1-es*) or 2 μM NA-PP1 (*mpk6SR*), and treated with 1 μM elf18 or water for the indicated time. For phos-tag gel assay using proteins produced in transgenic plants, 7-day-old seedlings grown on solid ½ MS were transferred to liquid ½ MS overnight before being treated with mock or 10 μM elf18 for the indicated time. The candidate proteins were extracted with modified extraction buffer [50 mM HEPES (pH 7.5), 50 mM KCl, 0.5% Triton-X

100, 1 mM DTT, 1× proteinase inhibitor cocktail (Roche)] and subjected to phos-tag gel analysis following the manufacturer's instructions. Briefly, the candidate proteins were analyzed using 8% (PAB8) or 6% (eIF4G and eIFiso4G1) SDS-polyacrylamide gels containing 40 μM $MnCl_2$ and 20 μM Phos-tag Acrylamide (FUJIFILM Wako). After electrophoresis, the gel was treated with the transfer buffer (20 mM Tris, 150 mM Glycine) containing 10 mM EDTA 3 times for 10 min each with gentle shaking and then one time without EDTA before protein transfer using the transfer buffer containing 0.05% SDS followed by immunoblotting.

### Antibody preparation

The phospho-specific antibodies against $PAB8^{S566}$, $eIF4G^{S1066/T1069}$, $eIFiso4G1^{S487}$ and $eIFiso4G1^{S542}$ were produced by Proteintech using the following peptides: Cys-GVHHRDS(p)PTSQPV (S566), Cys-KGLFPS(p)PHT(p)PMQVMH (S1066/T1069), Cys-SSGGPVS(p)PGPVYP (S487) and Cys-GPGPLHS(p)PAVSKS (S542).

### *In vitro* phosphorylation assay

Purified from *E. coli*, 200 ng MPK6-HIS was incubated with 2 μg GST-PAB8, GST-eIF4G or GST-eIFiso4G in 20 mL kinase reaction buffer [25 mM Tris-HCl (pH 7.5), 10 mM $MgCl_2$, 1 mM DTT, 100 mM ATP] at 30 °C for 30 min with $GST\text{-}PAB8^{S566A}$, $GST\text{-}eIF4G^{8A}$ and $GST\text{-}eIFiso4G1^{2A}$ as negative controls. The reaction was stopped by adding 4× SDS loading buffer and treated at 95 °C for 10 min. The phosphorylation of $PAB8^{S566}$, $eIF4G^{S1066/T1069}$, $eIFiso4G1^{S487}$ and $eIFiso4G1^{S542}$ were detected using anti-pS566, anti-pS1066/T1069, anti-pS487 and anti-pS542, antibodies, respectively.

### RNA-immunoprecipitation qPCR assay

*Arabidopsis* protoplasts were used for the transient expression of the FLAG-tagged PAB8 phospho-sites variants as previously described (Niu and Sheen, 2012) with modifications. In brief, 4 mL protoplasts (from 6-12 fully-expanded leaves digested in 4 mL enzyme solution) were transfected with 200 μg indicated plasmids and incubated overnight before treatment with 1% formaldehyde for 10 min. The cross-linking reaction was quenched by adding 125 mM Glycine for 5 min, followed by 2 times wash with W5 buffer. Samples were collected at 2,000 g for 30 sec and lysed with 900 μL of the lysis buffer [50 mM HEPES (pH 7.5), 100 mM KCl, 5 mM $MgCl_2$, 0.5% NP40, 1 mM DTT, 1× proteinase inhibitor cocktail (Roche), 200 U/mL RiboLock RNase Inhibitor (Thermo Scientific)]. After centrifuging at 16,000 g for 15 min, 200 μL of the supernatant was taken and treated with 2 mg/mL Proteinase K at 37 °C for 30 min to release RNAs cross-linked with proteins, followed by addition of 1 mL TRIzol and storage at -80 °C until further process (Input). The remaining supernatant was incubated with 5 μM oligos (5′-ACCAGAATTAGACTCAGAAGG-3′) targeting the *TBF1* mRNA to guide digestion by 6 U/mL RNAse H (Thermo Scientific) at 37 °C for 30 min to separate the 5′ fragment containing R-motifs from the 3′ poly (A) tail. The digested RNA sample was incubated with 50 μL agarose-conjugated anti-FLAG antibody (Sigma), which was prewashed 5 times with ice-cold NT2 buffer [50 mM HEPES (pH 7.5), 200 mM KCl, 2 mM EDTA, 0.05% NP40, 1 mM DTT, 40 U/mL RiboLock RNase Inhibitor] for 4 h at 4 °C with rotations. The precipitates were washed 5 times with the NT2 buffer and resuspended with 100 μL Proteinase K buffer [50 mM HEPES (pH 7.5), 150 mM NaCl, 6 mM EDTA, 0.5% SDS]. 2 mg/mL Proteinase K was added and incubated at 37 °C for 30 min to release RNAs (IP). The IP and Input RNA samples were subjected to 1 mL TRIzol extraction and reverse transcription using the First-strand cDNA Synthesis Kit (Thermo) following the manufacturer's manual before qPCR was performed using FastStart Universal SYBR Green Master Kit (Roche). The binding affinity of PAB8 to R-motif was measured by the ratio of IP RNA normalized to the Input RNA. The primers used are listed in Table S4.

## QUANTIFICATION AND STATISTICAL ANALYSIS

All experiments were repeated at least two times with similar results. Data plotting and statistical tests were performed using GraphPad Prism 8. Statistical information is embedded in the figure legends.

CellPress
OPEN ACCESS

# Supplemental figures

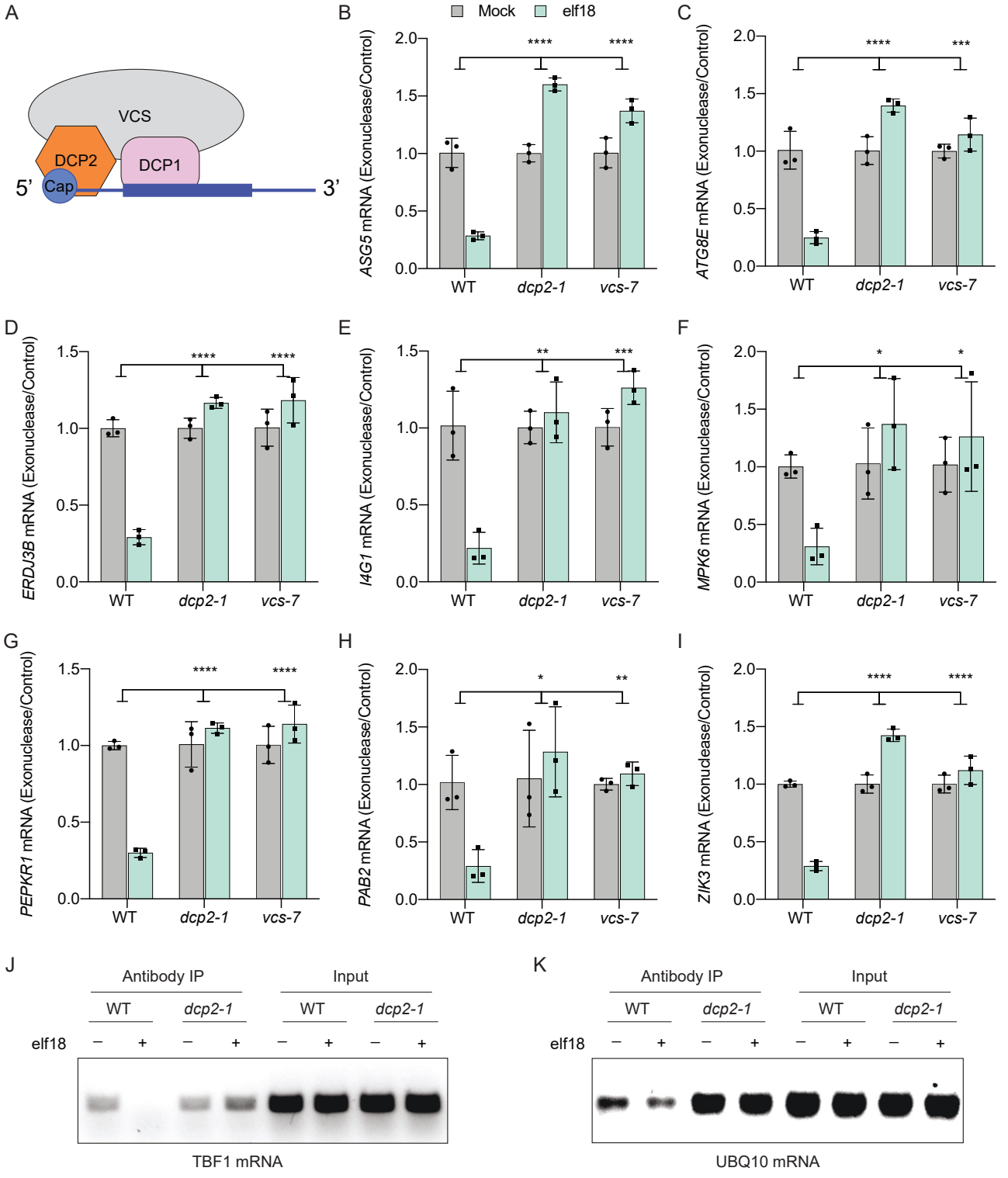


(legend on next page)

**Figure S1. Elf18-induced decapping of R-motif-containing genes, related to Figure 1**

(A) A cartoon of the decapping protein complex.

(B–I) Elf18-induced decapping of *ASG5* (B), *ATG8E* (C), *ERDJ3B* (D), *I4G1* (E), *MPK6* (F), *PEPKR1* (G), *PAB2* (H), and *ZIK3* (I) mRNAs was measured in 5-day-old seedlings after treatment with mock or 10 μM elf18 for 1 h. The extracted mRNAs were exposed to exonuclease before qPCR. Values are means ± SDs after normalizing to the unexposed control.

(J and K) Elf18-induced decapping of *TBF1* (J) and *UBQ10* (K) mRNAs *in planta*. The mRNAs extracted from 8-day-old seedlings after treatment with mock or 10 μM elf18 for 1 h were immunoprecipitated by an antibody against the cap structure before quantification by RT-PCR.

Each dot represents a biological replicate. Data were analyzed via two-way ANOVA, *$p < 0.05$, **$p < 0.01$, ***$p < 0.001$, ****$p < 0.0001$.

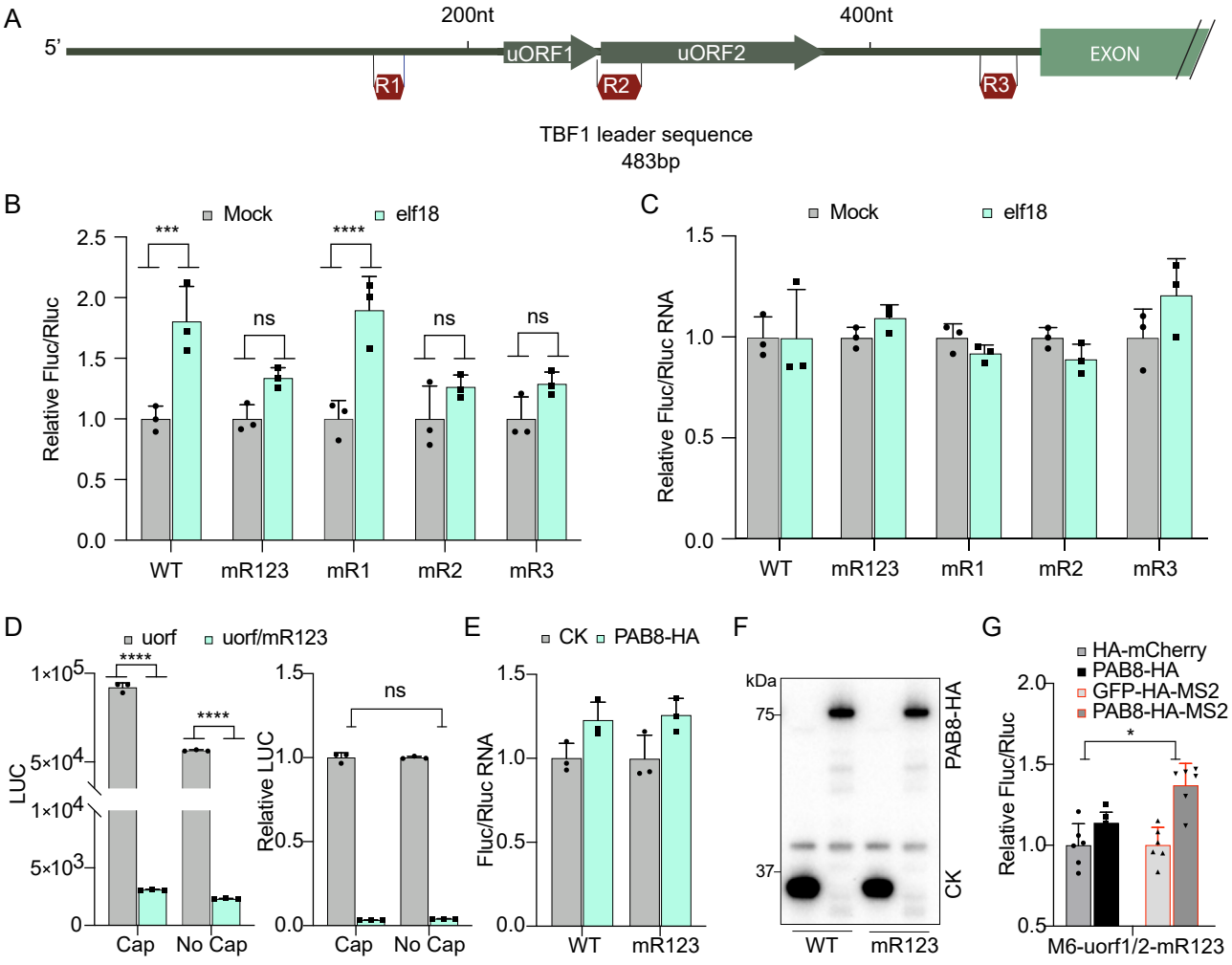


**Figure S2. R-motifs are required for elf18-induced cap-independent translation of *TBF1*, related to Figure 2**

(A) A schematic of the *TBF1* mRNA 5′ leader sequence. R, R-motif.

(B and C) *In planta* translation of *TBF1* reporters with WT or mutant R-motifs. The *35S:uORF/R$_{TBF1}$-FLUC/35S:RLUC* (WT) or the *35S:uORF/mRs$_{TBF1}$-FLUC/35S:RLUC* mutant (*mRs*) reporter was transiently coexpressed with the elf18 receptor EFR-GFP in *Nb* plants for 20 h before infiltration with 10 μM elf18 or water for 2 h. The relative luciferase activities (B) and luciferase mRNA levels (C) were measured. Values are means ± SDs.

(D) *In vitro* translational activities of capped and uncapped *uorf* or *uorf/mR123* mRNAs were measured using the wheat-germ translation system (left) and the relative fold changes calculated (right). Values are means ± SDs.

(E and F) For the experiment shown in Figure 2F, the FLUC/RLUC mRNA ratio was determined through qPCR (E) and the PAB8-HA protein level was examined by immunoblotting (F). Values are means ± SDs. CK, vector with the HA-mCherry.

(G) *In planta* translation of *uorf/mR123* using the MS2 tethering assay. The *35S:M6-uorf/mR123$_{TBF1}$-FLUC/35S:RLUC* dual luciferase reporter was transiently expressed with either MS2-tagged (GFP-HA-MS2 or PAB8-HA-MS2) or untagged proteins (HA-mCherry or PAB8-HA) in *Nb* plants for 2 days before luciferase activities were measured. Values are means ± SDs.

Each dot represents a biological replicate. Data were analyzed by two-way ANOVA with Dunnett multiple comparisons (B), t test (left D) and two-way ANOVA (right D and G), *p < 0.05, ***p < 0.001, ****p < 0.0001. ns, not significant.

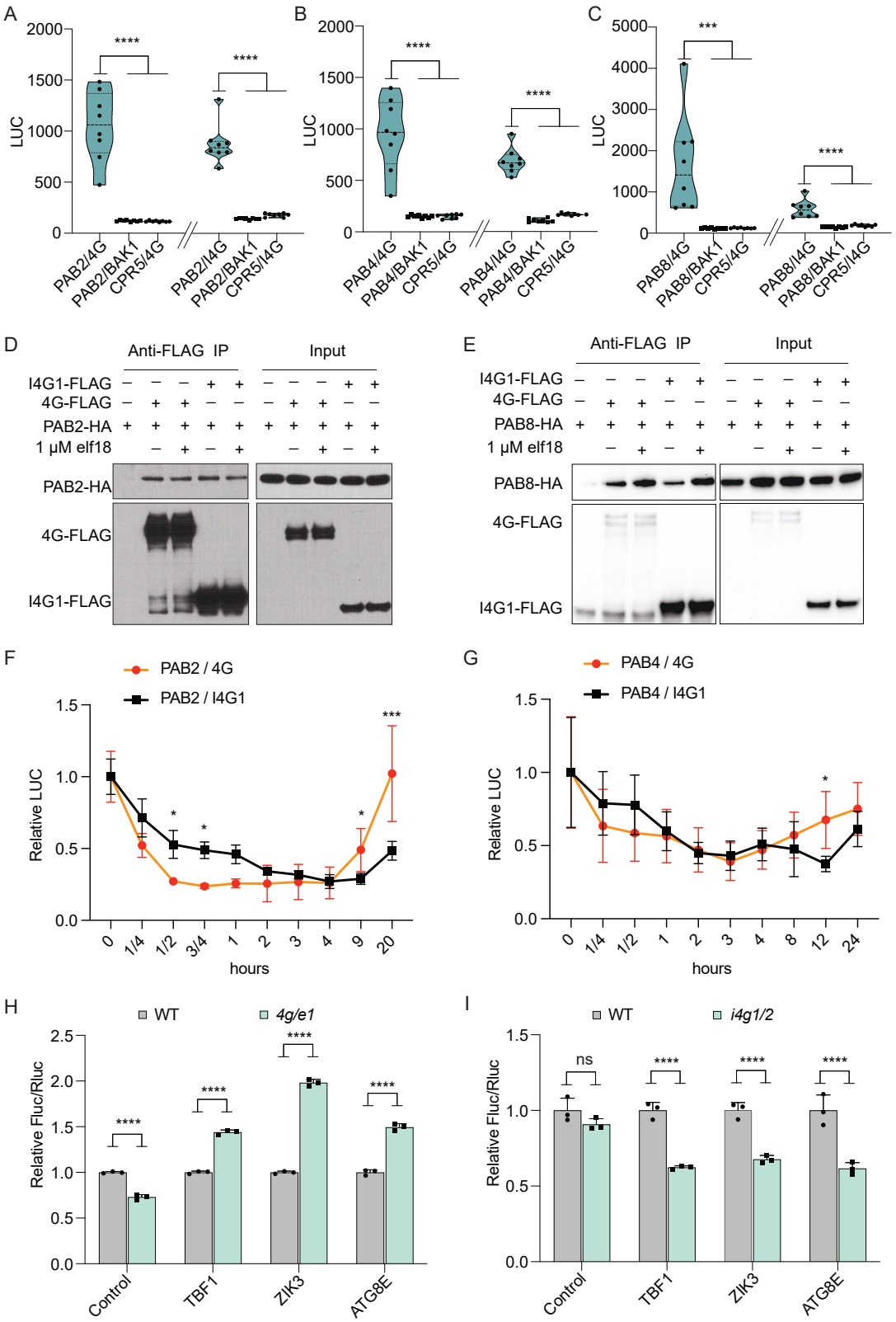


(legend on next page)

**Figure S3. PABPs dynamically interact with eIF4G and eIFiso4G, related to Figure 3**

(A–C) Split-luciferase assay. Cluc-tagged PABs and Nluc-tagged eIF4G (4G) or eIFiso4G1 (I4G1) were transiently coexpressed using the constitutive 35S promoter in *Nb* plants for 2 days to detect PAB2 (A), PAB4 (B), and PAB8 (C) interactions with eIF4G or eIFiso4G1. The unrelated Cluc-CPR5 and BAK1-Nluc were used as negative controls.

(D and E) Co-immunoprecipitation (coIP) assays were performed using agarose-conjugated anti-FLAG antibody after overnight coexpression of FLAG-tagged eIF4G (4G-FLAG) or eIFiso4G1 (I4G1-FLAG) with PAB2-HA (D) or PAB8-HA (E) in protoplasts treated with 1 μM elf18 for 10 min.

(F and G) The dynamics of the interaction between PAB2 (F) or PAB4 (G) and eIF4G (4G) or eIFiso4G1 (I4G1) upon elf18 treatment was determined using the split-luciferase assay after 10 μM elf18 or water treatment. Data are shown as the values (elf18/$H_2O$) normalized to time zero.

(H and I) Translation of R-motif-containing mRNAs, *TBF1*, *ZIK3*, and *ATG8E*, was measured using *TBF1*, *ZIK3*, and *ATG8E* 5′ leader sequences in dual luciferase reporters after overnight expression in protoplasts made from WT, *eif4g eif4e1* (*4g/e1*) (H), and *eifiso4g1 eifiso4g2* (*i4g1/2*) (I) plants. The *35S:FLUC/35S:RLUC* reporter was used as a control. Values are means ± SDs.

Each dot represents a biological replicate. Data were analyzed via one-way ANOVA (Tukey) (A–C, H, and I) and two-way ANOVA with Dunnett multiple comparisons (F and G), *$p < 0.05$, ***$p < 0.001$, ****$p < 0.0001$. ns, not significant.

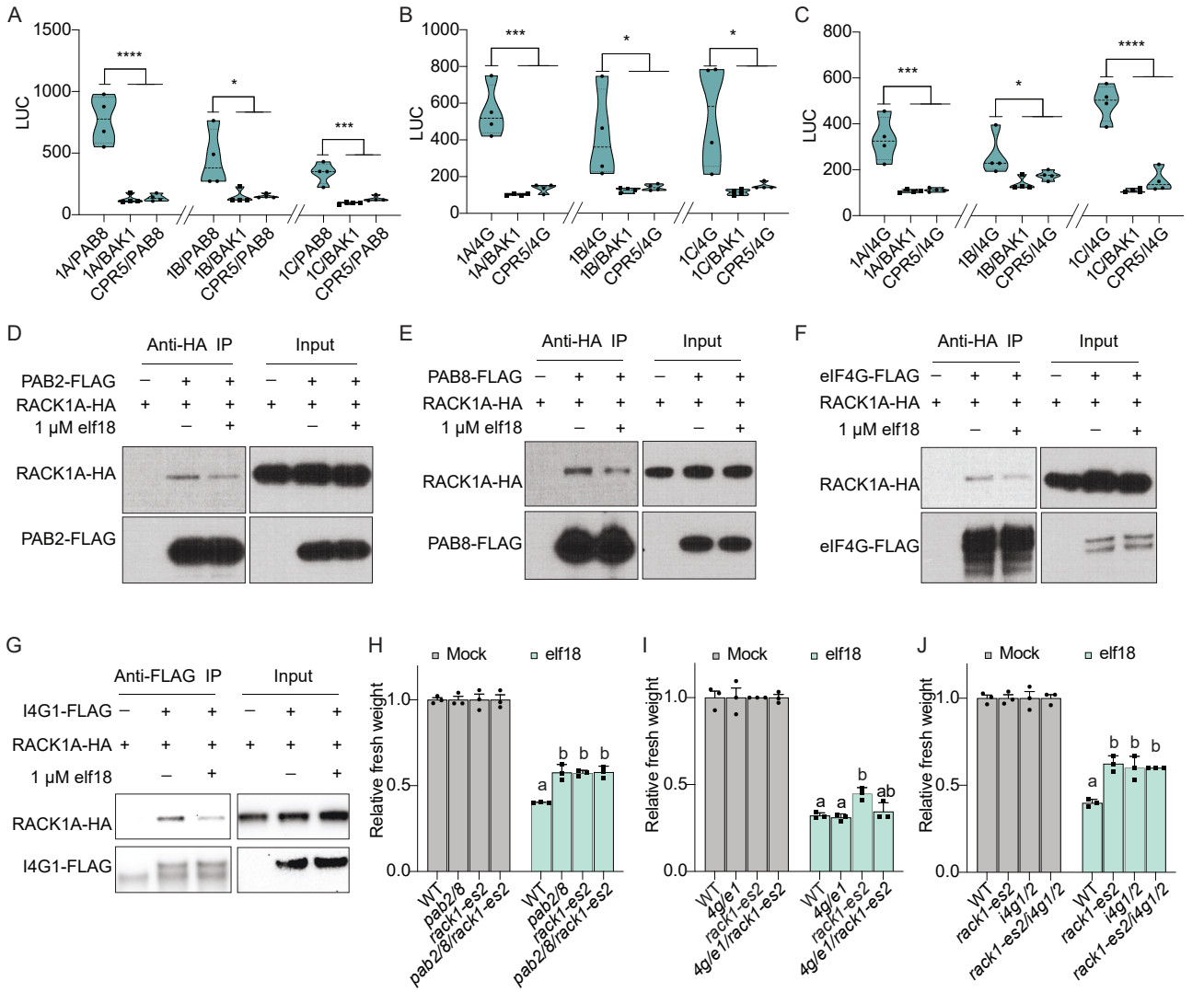


**Figure S4. PABP, RACK1, eIF4G, and eIFiso4G function together to regulate plant immunity, related to Figure 4**

(A–C) Split-luciferase assay. Cluc-tagged RACK1s (1A-1C) and Nluc-tagged PAB8, eIF4G (4G), or eIFiso4G1 (I4G1) were transiently coexpressed using the constitutive 35S promoter in *Nb* plants for 2 days to detect RACK1 interactions with PAB8 (A), eIF4G (B), or eIFiso4G (C). The unrelated Cluc-CPR5 and BAK1-Nluc were used as negative controls.

(D–G) Co-immunoprecipitation (coIP) assays were performed using agarose-conjugated anti-FLAG antibody after overnight coexpression of RACK1A-HA with FLAG-tagged PAB2 (D), PAB8 (E), eIF4G (F), or eIFiso4G1 (G) in protoplasts treated with 1 μM elf18 for 10 min.

(H–J) Elf18-associated growth inhibition. 5-day-old seedlings were treated with 50 μM estradiol overnight, then with mock or 100 nM elf18 for 3–4 days before fresh weight was measured in WT, *pab2 pab8* (*pab2/8*), *rack1-es2*, and *pab2/8/rack1-es2* (H); WT, *eif4g eif4e2* (*4g/e1*), *rack1-es2*, and *4g/e1/rack1-es2* (I); WT, *rack1-es2*, *eifiso4g1 eifiso4g2* (*i4g1/2*), and *rack1-es2/i4g1/2* (J). Values are means ± SEMs.

Each dot represents a biological replicate. Data were analyzed via one-way ANOVA (Tukey) (A–C) and two-way ANOVA with Dunnett multiple comparisons (H–J), *p < 0.05, ***p < 0.001, ****p < 0.0001, different letters indicate statistical significance. p < 0.05.

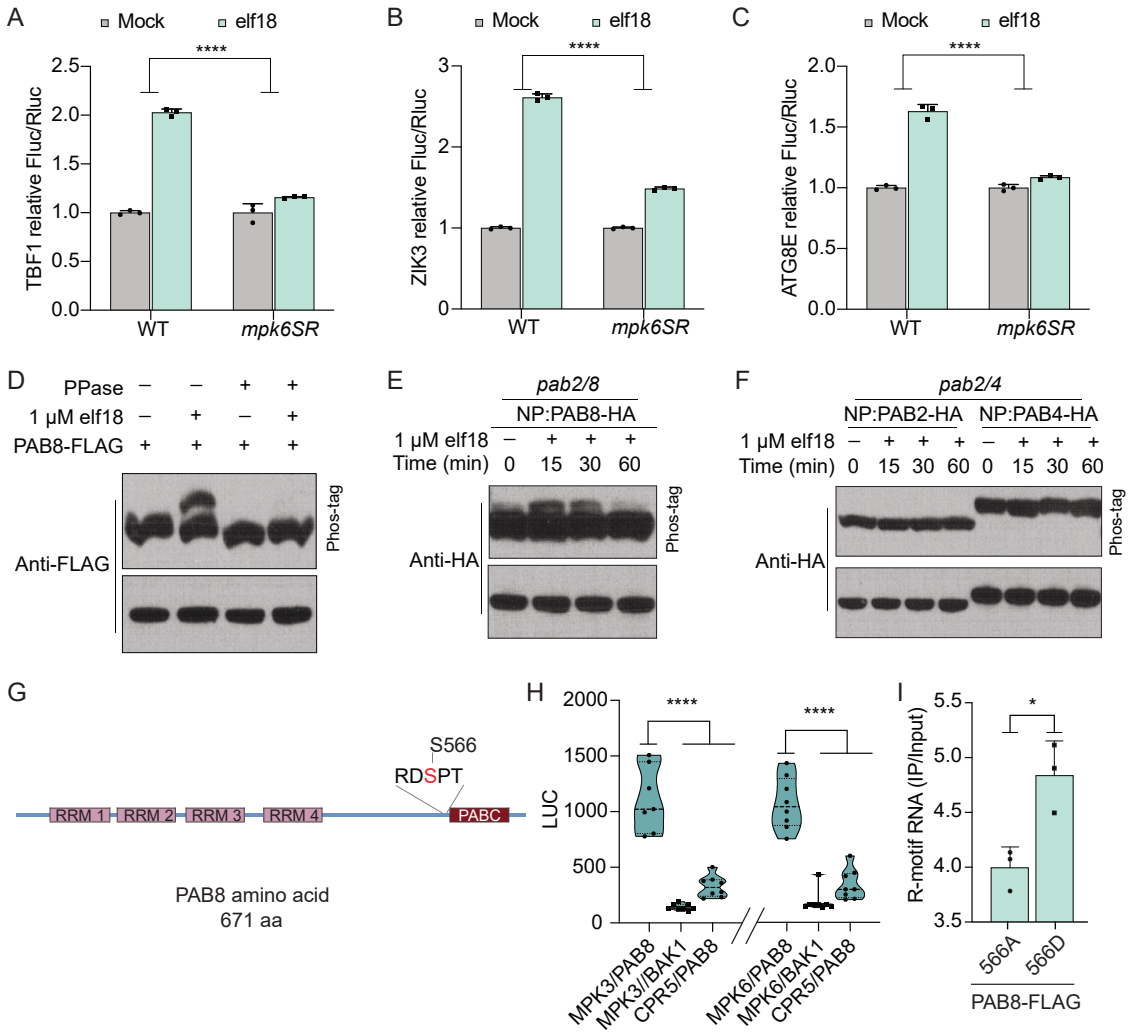


**Figure S5. Elf18 induces phosphorylation of PAB8, related to Figure 5**

(A–C) Elf18-induced translation of R-motif-containing mRNAs, *TBF1* (A), *ZIK3* (B), and *ATG8E* (C), was measured using *TBF1*, *ZIK3*, and *ATG8E* 5′ leader sequences in dual luciferase reporters after overnight expression in protoplasts made from WT and *mpk6SR* plants. The resulting protoplasts were treated with 1 μM elf18 for 45 min before the luciferase activities were measured. Values are means ± SDs.

(D) Confirmation of elf18-induced phosphorylation of PAB8 by protein phosphatase (PPase) treatment. PAB8-FLAG was extracted from protoplasts after treatment with 1 μM elf18 for 10 min. Protein samples with or without phosphatase treatment were examined using a phos-tag gel immunoblotted with an anti-FLAG antibody.

(E and F) Elf18-induced phosphorylation of PAB8 (E), PAB2, and PAB4 (F) in stable transgenic plants. 1-week-old seedlings were treated with 10 μM elf18 for the indicated time, and the mobility of HA-tagged PABPs was analyzed using a phos-tag gel immunoblotted with an anti-HA antibody.

(G) A schematic of the PAB8 protein with the phospho-site detected by LC-MS/MS. RRM, RNA recognition motif domain; PABC, poly(A)-binding protein C-terminal domain.

(H) Split-luciferase assay for MPK3/6 interaction with PAB8. Cluc-tagged MPKs and Nluc-tagged PAB8 were transiently coexpressed in *Nb* plants for 2 days before luciferase activities were measured. The unrelated Cluc-CPR5 and BAK1-Nluc were used as negative controls.

(I) Phosphodead (PAB8$^{S566A}$) and phosphomimetic (PAB8$^{S566D}$) PAB8 binding to *TBF1* R-motif *in vivo*. Protoplasts expressing PAB8$^{S566A}$ or PAB8$^{S566D}$ were treated with 1% formaldehyde for 10 min to cross-link PAB8 with R-motifs before lysis. The lysate was incubated with 5 μM oligos targeting the *TBF1* mRNA. RNAse H (0.006 U/μL) was added to separate the 5′ fragment containing R-motifs from the 3′ poly(A) tail, followed by RNA-immunoprecipitation-qPCR to quantify the binding between PAB8 and R-motifs.

Each dot represents a biological replicate. Data were analyzed by two-way ANOVA (A–C), one-way ANOVA (Tukey) (H), and t test (I), *p < 0.05, ****p < 0.0001.

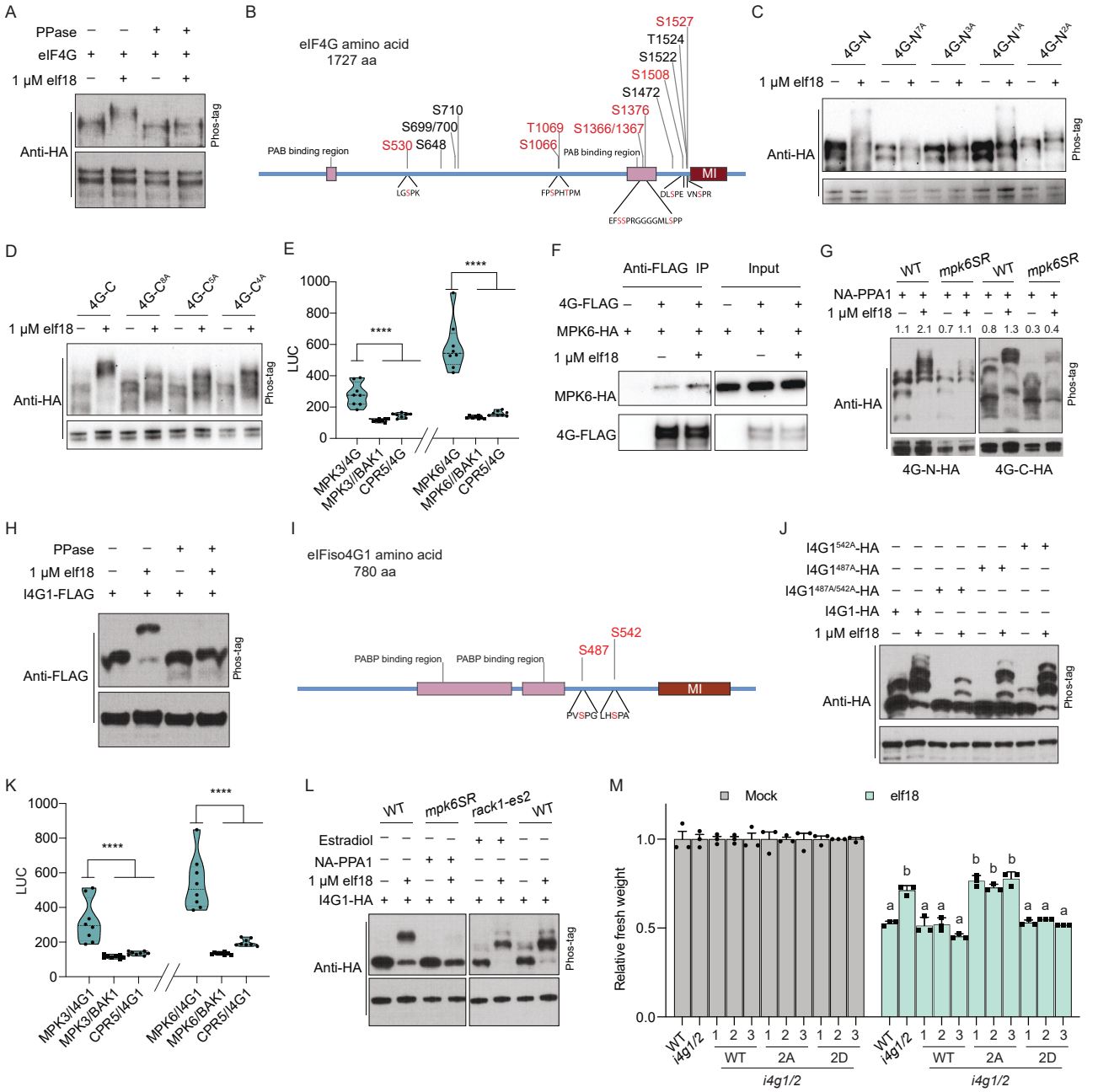


**Figure S6. Elf18-induced eIF4G and eIFiso4G phosphorylation by MPK3/6, related to Figure 6**

(A) Confirmation of elf18-induced phosphorylation of eIF4G by protein phosphatase (PPase) treatment. eIF4G-HA was extracted from protoplasts after treatment with 1 μM elf18 for 10 min. Protein samples with or without phosphatase treatment were examined using a phos-tag gel immunoblotted with an anti-HA antibody.

(B) A schematic of the eIF4G protein with phospho-sites identified by LC-MS/MS. Sites with a typical MPK3/6 phosphorylation motif are highlighted in red. MI: a protein-protein interaction domain.

(C) Ser530, Ser1066, and Thr1069 as major phospho-sites in the N-terminal half of eIF4G-HA (4G-N). 4G-N and serine-to-alanine mutants were analyzed as in (A). 7A: S530A, S648A, S699A, S700A, S710A, S1066A, and T1069A; 3A: S530A, S1066A, and T1069A; 1A: S530A; 2A: S1066A and T1069A.

(D) Ser1366, Ser1367, Ser1376, Ser1508, and Ser1527 as major phospho-sites in the C-terminal half of eIF4G-HA (4G-C). Experiment was performed as in (A). 8A: S1366A, S1367A, S1376A, S1472A, S1508A, S1522A, T1524A, and S1527A; 5A: S1366A, S1367A, S1376A, S1508A, and S1527A; 4A: S1366A, S1367A, S1376A, and S1527A.

(E) Spit luciferase assay for MPK3/6 interaction with eIF4G. Cluc-tagged MPKs and Nluc-tagged eIF4G were transiently coexpressed in *Nb* plants for 2 days before luciferase activities were measured. The unrelated Cluc-CPR5 and BAK1-Nluc were used as negative controls.

(F) Co-immunoprecipitation (coIP) assay for eIF4G interaction with MPK6. CoIP assay was performed using an agarose-conjugated anti-FLAG antibody for eIF4G-FLAG (4G-FLAG) and MPK6-HA isolated from protoplasts after treatment with 1 μM elf18 for 10 min.

*(legend continued on next page)*

(G) Elf18-induced phosphorylation of eIF4G by MPK3/6. 4G-N-HA and 4G-C-HA were expressed in WT or *mpk6SR* (inhibitor-sensitized MPK3 variant-rescued *mpk3 mpk6* double mutant) protoplasts in the presence of 2-μM NA-PP1 and analyzed as in (A).

(H) Confirmation of elf18-induced phosphorylation of eIFiso4G1 by protein phosphatase (PPase) treatment. eIFiso4G1-FLAG (I4G1-FLAG) was extracted from protoplasts after treatment with 1 μM elf18 for 10 min. Mobility change of the protein samples with or without phosphatase treatment was examined using a phos-tag gel immunoblotted with an anti-FLAG antibody.

(I) A schematic of the eIFiso4G1 protein with phospho-sites detected by LC-MS/MS. MI: a protein-protein interaction domain.

(J) Ser487 and Ser542 as the major phospho-sites in eIFiso4G1 upon elf18 treatment. eIFiso4G1 (I4G1-HA) and serine-to-alanine single ($I4G1^{487A}$-HA and $I4G1^{542A}$-HA) and double ($I4G1^{487A/542A}$-HA) mutants were analyzed as in (A) with an anti-HA antibody.

(K) Split-luciferase assay for MPK3/6 interaction with eIFiso4G1 was performed as in (E).

(L) Elf18-induced phosphorylation of eIFiso4G1 by MPK3/6. eIFiso4G1-HA (I4G1-HA) was expressed in WT, *mpk6SR*, and *rack1-es2* protoplasts in the presence of 2-μM NA-PP1 inhibitor (*mpk6SR*) and 50 μM estradiol (*rack1-es2*) and analyzed as in (A) with an anti-HA antibody.

(M) Elf18-associated growth inhibition. 5-day-old independent *Arabidopsis* transgenic lines in the *eifiso4g1 eifiso4g2* (*i4g1/2*) expressing *NP:eIFiso4G1-HA* (WT), *NP:eIFiso4G1*$^{S487A/S542A}$*-HA* (2A), or *NP:eIFiso4G1*$^{S487D/S542D}$*-HA* (2D) were treated with mock or 100 nM elf18 for 3–4 days before fresh weight was measured. *NP*, eIFiso4G1 native promoter. Values are means ± SDs.

Each dot represents a biological replicate. Data were analyzed by one-way ANOVA (Tukey) (E and K) and two-way ANOVA with Dunnett multiple comparisons (M), different letters indicate statistical significance, $p < 0.05$; ****$p < 0.0001$.